

Large Stark Effect for Li Donor Spins in Si

Luke Pendo,¹ E.M. Handberg,¹ V.N. Smelyanskiy,² and A.G. Petukhov^{1,*}

¹*Physics Department, South Dakota School of Mines and Technology, Rapid City, SD 57701*

²*NASA Ames Research Center, Mail Stop 269-1, Moffett Field, CA 94043*

(Dated: August 7, 2018)

We study the effect of a static electric field on lithium donor spins in silicon. The anisotropy of the effective mass leads to the anisotropy of the quadratic Stark susceptibility, which we determined using the Dalgarno-Lewis exact summation method. The theory is asymptotically exact in the field domain below Li-donor ionization threshold, relevant to the Stark-tuning electron spin resonance experiments. To obtain the generalized Stark susceptibilities at arbitrary fields, we propose a new variational wave function which reproduces the exact results in the low-field limit. With the calculated susceptibilities at hand, we are able to predict and analyze several important physical effects. First, we observe that the energy level shifts due to the quadratic Stark effect for Li donors in Si are equivalent to, and can be mapped onto, those produced by an external stress. Second, we demonstrate that the Stark effect anisotropy, combined with the unique valley-orbit splitting of a Li donor in Si, spin-orbit interaction and specially tuned external stress, may lead to a very strong modulation of the donor spin g -factor by the electric field. Third, we investigate the influence of random strains on the g -factor shifts and quantify the random strain limits and requirements to Si material purity necessary to observe the g -factor Stark shifts experimentally. Finally, we discuss possible implications of our results for quantum information processing with Li spin qubits in Si.

PACS numbers: 71.70.Ej, 71.55.-I, 71.55.Ak, 76.30.-v, 03.67.-a, 03.67.Lx

I. INTRODUCTION

Recent research has shown that electron spins bound to donors in Si are some of the most viable candidates for scalable, solid-state quantum computing applications¹. The lithium donor is unique among other Si shallow donors² because its ground state is degenerate.^{3,4} We will demonstrate that the inverted electronic structure of the lithium donor allows intriguing possibilities for the efficient manipulation of Li spin qubits using stress and electric fields. The ability to couple individual electron spins with local electric fields is a key feature of many spin-control proposals for quantum computing and single-electron spintronic applications.^{1,5-12} The electrical control of single electron spins based on various coupling mechanisms has been demonstrated experimentally for semiconductor quantum dots.¹³⁻¹⁷ Also, a possibility of spin-orbit-driven electrical modulation of shallow donor g -factors in GaAs has been predicted theoretically.¹⁸ In this work, we present theoretical evidence that the Li donor in Si is yet another shallow donor system that possesses such functionality. This system may play a significant role in silicon-based quantum information processing (QIP) with spin qubits.

The Stark effect for shallow donors in silicon has been studied both experimentally¹⁹ and theoretically.²⁰⁻²² Most of the theoretical calculations have been performed for substitutional donors (e.g. P)²⁰ but not for Li donors occupying tetrahedral interstitials in a silicon lattice.³ Furthermore, most of the previous studies of substitutional donors ignore the interplay between the Stark and Zeeman effects. This interplay occurs because the spin-orbit interaction couples the non-degenerate ground state of a substitutional donor to the rest of 1s manifold,^{23,24}

which is separated from the ground state by large valley-orbit splitting, $\Delta_{vo} \sim 10$ meV. Since the spin-orbit coupling is much smaller than Δ_{vo} , the electrical modulation of the g -factors of substitutional donors is strongly suppressed. On the contrary, the ground state of the interstitial Li donor is degenerate and even modest spin-orbit interaction may have a profound effect on the energy levels leading to a strong electric field dependence of the Zeeman splittings.

Intriguingly, the orbital degeneracy of the ground state quintet of the lithium donor gives rise not only to non-trivial spin-orbit effects³ but also to a strong long-range *elastic-dipole* coupling between the orbital states of different lithium donors.² The elastic-dipole coupling was studied earlier in connection to an acceptor-based quantum computing scheme in silicon proposed by Dykman and Golding²⁵. Thus, it is of interest to study the lithium donor electron as a new candidate for QIP applications with a long-range inter-donor coupling.

Experimental techniques utilizing pulsed electron spin resonance (ESR) measurements in interdigitated devices based on Sb-doped Si revealed observable Stark shifts of ESR lines in an electric field \mathcal{E} . The shifts can be parametrized as $\Delta A/A = \eta_a \mathcal{E}^2$ and $\Delta g/g = \eta_g \mathcal{E}^2$, for the hyperfine constant and the g -factor shifts respectively, where $\eta_a \approx -3.7 \times 10^{-3} \mu\text{m}^2/\text{V}^2$ and $\eta_g \approx -1 \times 10^{-5} \mu\text{m}^2/\text{V}^2$.¹⁹ We anticipate that experiments on similar devices based on Li-doped Si may reveal substantially larger shifts of the magnetic resonance lines on the order of 10 gauss for electric fields ranging from 0 to 3 kV/cm. This proposition seems somewhat surprising as there is no hyperfine interaction in the ground state for Li donors and the strength of the spin-orbit interaction on the Li atom in Si is negligible.³ Nonetheless,

spin-orbit effects have been observed quite prominently in ESR spectra of Li-doped natural Si under external stress.³

This happens because the unique electronic structure of a Li donor enables observation of spin-orbit effects which have *crystalline* rather than impurity origin.³ The situation in P-doped Si is quite different because the crystalline spin-orbit interaction is much less important due to its weak influence on the isolated, non-degenerate ground state. More specifically, the orbital states of the $1s$ manifold of a shallow donor in silicon form a singlet A_1 , a doublet E and a triplet T_2 . For substitutional donors the singlet ground state A_1 is separated by a gap exceeding 10 meV from the closely spaced doublet and triplet. The sequence of levels is inverted for the interstitial Li donors in such a way that the ground state is five-fold degenerate and composed of the orbital doublet $1s(E)$ and triplet $1s(T_2)$ while the singlet $1s(A_1)$ lies 1.76 meV above (see Fig. 1).

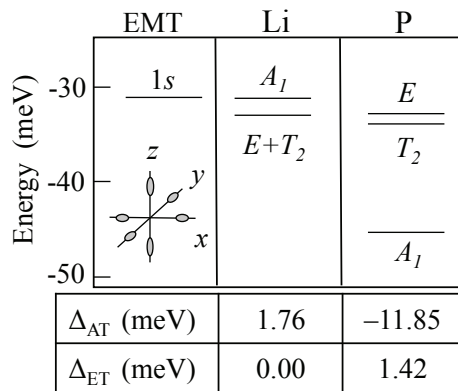


FIG. 1. Upper table shows the energy level diagrams for $1s$ electron of the shallow donors in silicon: left column corresponds to EMT calculations giving the binding energy 31.27 meV.²⁶ Experimental values for the $1s$ energies of substitutional phosphorus²⁷ and interstitial lithium⁴ donors are shown in right and middle columns, respectively. Ionization energy of lithium donor 33.02 meV is in particularly close agreement with EMT result. Inset depicts the locations of 6 conduction band minima in silicon. Lower table shows the experimental results for the energy differences between the singlet and triplet (Δ_{AT}) and between the doublet and triplet (Δ_{ET}).

Within the Effective Mass Theory (EMT) the $1s$ donor electron manifold has 6-fold orbital degeneracy corresponding to 6 minima of the silicon conduction band \mathbf{k}_{sj} . These minima are located along coordinate axes at about 85% of the distance to the zone boundary as shown in the inset of Fig. 1:

$$\mathbf{k}_{sj} = s\kappa_0 \mathbf{n}_j, \quad s = \pm 1, \quad \kappa_0 \approx 0.85 G_{100}/2, \quad (1)$$

where \mathbf{n}_j is a Cartesian unit vector, $j = x, y$ or z , $G_{001} = 4\pi/a_0$ is a magnitude of the reciprocal lattice vector in $[001]$ direction, and a_0 is the Si lattice constant. The

position of each valley is characterized by a composite index $\{sj\}$, where $s = \pm 1$ describes the valley centered on either the positive or the negative semi-axis, respectively.

A short-range tetrahedral potential corresponding to the local symmetry of the donor site splits the valley degeneracy. The intervalley effects²⁸ are described by the valley-orbit Hamiltonian

$$H_{vo} = (E_0 + \Delta_0) \sum_{i,s} |si\rangle \langle si| + \Delta_1 \sum_{s,i} |si\rangle \langle -si| + \Delta_2 \sum_{i,j,s,s'} (1 - \delta_{ij}) |si\rangle \langle s'j|. \quad (2)$$

Here, E_0 is the binding energy corresponding to the solution of the single-valley Coulomb problem and the parameters Δ_i are the matrix elements of the short-range central cell potential in the basis of the six valley orbitals

$$\langle \mathbf{r} | sj \rangle = \exp(i\mathbf{k}_{sj} \cdot \mathbf{r}) u_{sj}(\mathbf{r}) F_{sj}(\mathbf{r}), \quad (3)$$

where $u_{sj}(\mathbf{r})$ is a periodic part of the Bloch function corresponding to the center of the valley \mathbf{k}_{sj} , and $F_{sj}(\mathbf{r})$ is the $1s$ envelope function which, along with E_0 , is found by solving the single-valley Coulomb problem.

The six eigenstates of the Hamiltonian (2), referred to as *symmetrized valley orbitals*, can be expressed as

$$|\mu\rangle = \sum_{s,j} \alpha_{sj}^\mu |sj\rangle, \quad \mu = 1, \dots, 6. \quad (4)$$

Each orbital $|\mu\rangle$ in Eq. (4) belongs to the irreducible representation μ of the tetrahedral group T_d characterized by the valley-orbit coefficients α_{sj}^μ that are given in Table I.

The singlet state A_1 and the doublet states E_θ , E_ϵ are “even” with respect to the axis inversion, i.e. they are symmetric combinations of the opposite valley orbitals, $\alpha_{sj} = \alpha_{-sj}$. On the contrary, each triplet state T_{2j} ($j=x, y$ or z) is an “odd” antisymmetric combination of just two opposite valleys orbitals, $\alpha_{sj} = -\alpha_{-sj}$. We have labeled the symmetrized valley orbitals according to Watkins and Ham³ and indicated their transformational properties under the group T_d (last column in Table I). Thus the singlet, triplet and doublet states possess s , p and d -like characters, respectively.

For phosphorus donors in silicon, Friesen²⁰ discussed two competing mechanisms which determine the behavior of the electron levels in the $1s$ manifold. First, as the electric field is increased, the quadratic Stark shift causes the energy of each valley to decrease. This will influence the form of the valley-orbit Hamiltonian (2). Formally, we have to replace E_0 with valley-dependent terms $E_{0i} = E_0 - \delta_i(\mathcal{E})$ and place these under the summation sign in Eq. (2), where the corrections δ_i include the quadratic Stark shifts of each valley. Secondly, similar substitutions are required for the central cell terms in the Hamiltonian $\Delta_0 \rightarrow \Delta_{0i}$, $\Delta_1 \rightarrow \Delta_{1i}$ and $\Delta_2 \rightarrow \Delta_{2ij}$. These parameters Δ are the matrix elements of the short-range central cell potential between the states $|is\rangle$; they

| μ -states | valley-orbit coefficients $\{\alpha_{sj}^\mu\}$ | basis functions | |
|---------------|---|---|-----------------------|
| 1 | A_1 | $\frac{1}{\sqrt{6}}(1, 1, 1, 1, 1, 1)$ | $x^2 + y^2 + z^2$ |
| 2 | E_θ | $\frac{1}{\sqrt{12}}(-1, -1, -1, -1, 2, 2)$ | $2z^2 - x^2 - y^2$ |
| 3 | E_ϵ | $\frac{1}{2}(1, 1, -1, -1, 0, 0)$ | $\sqrt{3}(x^2 - y^2)$ |
| 4 | T_{2x} | $\frac{1}{\sqrt{2}}(1, -1, 0, 0, 0, 0)$ | x |
| 5 | T_{2y} | $\frac{1}{\sqrt{2}}(0, 0, 1, -1, 0, 0)$ | y |
| 6 | T_{2z} | $\frac{1}{\sqrt{2}}(0, 0, 0, 0, 1, -1)$ | z |

TABLE I. Table of valley-orbit coefficients for silicon donor $1s$ orbital states. First column defines the order of states. Second column shows the state label derived from the corresponding representation of the group T_d . Each row in the third column gives a set of 6 coefficients $\{\alpha_{sj}\}$ for $sj=\pm 1, \pm 2, \pm 3$ corresponding to the silicon conduction valley minima at $\pm x, \pm y, \pm z$ axes, respectively. Fourth column shows basis functions describing the transformational properties of the corresponding states under the operations of the group T_d

are proportional to the amplitudes of the envelope functions $F_{sj}(0)$ in the central cell. Since the electric field \mathcal{E} pulls the electron away from the donor site, the amplitudes $F_{sj}(0)$ and the matrix elements Δ are decreasing functions of \mathcal{E}^2 . As a result, the energy spectrum of the manifold narrows and the ground state shifts upward in the direction opposite to the quadratic Stark shift.

Our studies reveal that the narrowing effect is not as important for Li as for P donors. Because the valley-orbit splitting for Li is considerably smaller than phosphorus, the narrowing of the spectrum does not overwhelm the quadratic Stark effect in determining the overall behavior of the $1s$ manifold in the presence of an electric field. According to our findings, the most important effect for Li is the anisotropy of the quadratic Stark effect. This anisotropy allows the electric field to induce unique splitting of the Li ground state and leads to a very non-trivial interplay of the Zeeman and Stark effects.

Our approach utilizes the Dalgarno-Lewis exact summation method to determine the quadratic Stark susceptibility. While this calculation is quite lengthy, it provides us with an important calibration tool to further devise our variational function in the presence of the electric field and gauge it against the exact small-field asymptotic behavior. We will discuss how the ground state splitting caused by the electric field can replicate stress effects and can potentially be used to manipulate a Li spin qubit. While most of the theoretical papers on the Stark effect were concerned with rather large fields,^{21,29-31} our studies are focused on the field domain below the 3-5 kV/cm relevant to the ESR Stark experiments, i.e. below ionization threshold of shallow donors in Si.

The paper is organized as follows. In Section II we study the quadratic Stark effect for a single-valley Schrödinger equation for a shallow donor in Si. The goal of this section is to calculate the Stark susceptibility, which is asymptotically exact in the limit of low electric fields using an exact summation method of Dal-

garno and Lewis tailored to account for the effective mass anisotropy. Based on the findings of Section II, we propose a new variational wave function in Section III. This wave function not only replicates the exact susceptibility at low fields but also describes the off-center displacement of the probability maximum for intermediate and high electric fields. In Sections IV-V, we introduce valley-orbit and external stress effects, and in Section VI, we describe the spin-orbit and Zeeman Hamiltonians. In Section VII, based on the results of the previous sections, we calculate the electric-field-induced ESR g -factor shifts for various types of spin-flip transitions and analyze the effects of random strains on the Stark shifts of the ESR spectra. Section VIII contains the summary and conclusions.

II. QUADRATIC STARK EFFECT

As a first step let us consider a quadratic Stark effect for a single-valley donor. We start with the EMT Kohn-Luttinger Hamiltonian²⁸ perturbed by an external electric field \mathcal{E}

$$H_z = -\frac{\hbar^2}{2m_\perp} \left(\frac{\partial^2}{\partial x^2} + \frac{\partial^2}{\partial y^2} + \gamma \frac{\partial^2}{\partial z^2} \right) - \frac{e^2}{\kappa r} - e\mathcal{E} \cdot \mathbf{r}, \quad (5)$$

where κ is the dielectric constant, $\gamma = m_\perp/m_\parallel$ is the effective mass anisotropy parameter, m_\perp and m_\parallel are transverse and longitudinal effective masses respectively, and we assume that the heavy-mass axis of the valley is along z . For our purposes it is convenient to rewrite the Hamiltonian (5) using a scaling transformation $z \rightarrow \sqrt{\gamma}z$. This yields

$$H_{z\rho} = -\frac{\hbar^2}{2m_\perp} \left(\frac{\partial^2}{\partial x^2} + \frac{\partial^2}{\partial y^2} + \frac{\partial^2}{\partial z^2} \right) - \frac{e^2}{\kappa\rho} - e\mathcal{E} \cdot \boldsymbol{\rho}, \quad (6)$$

where $\boldsymbol{\rho} = (x, y, \sqrt{\gamma}z)$.

Our immediate goal is to find a second order shift of the ground state energy produced by an external static electric field \mathcal{E} (Stark shift):

$$\begin{aligned} \delta_z(\mathcal{E}) &= \sum_{n \neq 1s} \frac{\langle 1s | e\mathcal{E} \cdot \boldsymbol{\rho} | n \rangle \langle n | e\mathcal{E} \cdot \boldsymbol{\rho} | 1s \rangle}{E_{1s} - E_n} \\ &= -\frac{1}{2} \chi_{\alpha\beta} \mathcal{E}_\alpha \mathcal{E}_\beta, \end{aligned} \quad (7)$$

where we introduced the Stark susceptibility tensor and assumed summation over repeating Greek indices. In the chosen coordinate system, the tensor $\chi_{\alpha\beta}$ is diagonal and has only two distinct components $\chi_{zz} = \chi_\parallel$ and $\chi_{xx} = \chi_{yy} = \chi_\perp$ due to the axial symmetry of the valley with respect to z .

It is well known from the classical problem of the quadratic Stark effect in a hydrogen atom that any perturbative treatment of the hydrogen Schrödinger equation in an external electric field requires summation of infinite series to account for the excited states of the continuous spectrum.³²⁻³⁵ To accomplish this for the lithium

donor, we will utilize the Dalgarno-Lewis exact summation method³⁶. We define a vector function $\mathbf{f}(\mathbf{r})$ to satisfy the equation

$$[\mathbf{f}(\mathbf{r}), H] |1s\rangle = -\boldsymbol{\rho} |1s\rangle. \quad (8)$$

With this equation in hand, consider an important condition for computing the second-order summation:

$$\begin{aligned} \langle n | \boldsymbol{\rho} | 1s \rangle &= -\langle n | [\mathbf{f}, H] | 1s \rangle \\ &= (E_n - E_{1s}) \langle n | \mathbf{f} | 1s \rangle. \end{aligned} \quad (9)$$

As a consequence, if the solution $\mathbf{f}(\mathbf{r})$ of Eq. (8) is known, the Stark susceptibility tensor defined in Eq. (7) can be obtained as

$$\chi_{\alpha\beta} = 2e^2 \langle 1s | r_\alpha \cdot f_\beta(\mathbf{r}) | 1s \rangle. \quad (10)$$

As both, the potential terms of H , as well as $\mathbf{f}(\mathbf{r})$ are functions of the coordinates only, they will commute and thus $[\mathbf{f}, H] = -(\hbar^2/2m_\perp) [\mathbf{f}, \nabla^2]$. Expressed in the coordinate-representation, Eq. (8) becomes a differential equation defining the function $\mathbf{f}(\mathbf{r})$ such that

$$\nabla^2 \mathbf{f}(\mathbf{r}) + 2(\boldsymbol{\xi} \cdot \nabla) \mathbf{f}(\mathbf{r}) = -\frac{2m_\perp}{\hbar^2} \boldsymbol{\rho}, \quad (11)$$

where $\boldsymbol{\xi} = \nabla \ln(\psi_{1s})$, and $\psi_{1s}(\mathbf{r}) \equiv \langle \mathbf{r} | 1s \rangle$ is the ground state wave function.

To describe the ground state wave function $\psi_{1s}(\mathbf{r})$ we use the Kohn-Luttinger function^{26,28} with ellipsoidal symmetry,

$$\psi_{1s}(\mathbf{r}) = \frac{\beta^{1/4}}{(\pi a_\perp^3)^{1/2}} \exp\left(-\frac{\sqrt{x^2 + y^2 + \beta z^2}}{a_\perp}\right), \quad (12)$$

where $\beta = \gamma a_\perp^2 / a_\parallel^2$ and a_\perp, a_\parallel are the transverse and longitudinal radii of the isolated valley in the absence of the electric field. Then

$$\boldsymbol{\xi} = -\frac{1}{a_\perp} \frac{x\hat{x} + y\hat{y} + \beta z\hat{z}}{\sqrt{x^2 + y^2 + \beta z^2}}. \quad (13)$$

At this point it is convenient to introduce another scaling transformation such that $x \rightarrow a_\perp x$, $y \rightarrow a_\perp y$, and $z \rightarrow a_\perp z / \sqrt{\beta}$. Under this transformation all the coordinates become dimensionless (measured in units of a_\perp) and the ground state wave function $\psi_{1s} \rightarrow \exp(-r) / \sqrt{\pi}$.

Also, in Eq. (11) we explicitly separate the anisotropic term proportional to $\lambda = 1 - \beta$ and treat it as a perturbation (i.e. we will construct our solution as a power series in the anisotropy parameter λ). This yields:

$$\hat{D}_r \mathbf{f} - \lambda \hat{D}_z \mathbf{f} = -\frac{2m_\perp a_\perp^3}{\hbar^2} \boldsymbol{\zeta}, \quad (14)$$

where $\boldsymbol{\zeta} = (x, y, z\sqrt{\gamma/\beta})$, and

$$\hat{D}_r = \nabla^2 - 2\partial/\partial r, \quad (15a)$$

$$\hat{D}_z = \partial^2/\partial z^2 - 2(z/r)\partial/\partial z. \quad (15b)$$

From the axial symmetry of Eq. (14), we are looking for solutions in the form:

$$f_x(\mathbf{r}) = (a_\perp/E_\perp) \cos\phi \cdot f_\perp(r, \theta), \quad (16a)$$

$$f_y(\mathbf{r}) = (a_\perp/E_\perp) \sin\phi \cdot f_\perp(r, \theta), \quad (16b)$$

$$f_z(\mathbf{r}) = (a_\parallel/E_\perp) \cdot f_\parallel(r, \theta), \quad (16c)$$

where $E_\perp = \hbar^2/2m_\perp a_\perp^2$ and $a_\parallel = a_\perp \sqrt{\gamma/\beta}$. The partial differential equation (14) may be further simplified by generating a coupled system of ordinary differential equations. The explicit angular dependence of the operators \hat{D}_r and \hat{D}_z is presented and analyzed in Appendix A. The analysis suggests that $f_\parallel(r, \theta)$ and $f_\perp(r, \theta)$ can be expanded into series in Legendre's and associated Legendre's polynomials, respectively, as follows:

$$f_\parallel(r, \theta) = \sum_{l=1} f_{\parallel,l}(r) P_l(\cos\theta), \quad (17a)$$

$$f_\perp(r, \theta) = -\sum_{l=1} f_{\perp,l}(r) P_l^1(\cos\theta). \quad (17b)$$

Note that the series expansion begins at $l = 1$.

Substituting the Legendre's expansions (17a) and (17b) into Eqs (16a)-(16c), inserting the results into Eq. (10) for the Stark susceptibility tensor, and integrating over the angular variables we obtain:

$$\chi_\parallel = \frac{8e^2 a_\parallel^2}{3E_\perp} \int_0^\infty r^3 \exp(-2r) f_{\parallel,1}(r) dr, \quad (18a)$$

$$\chi_\perp = \frac{8e^2 a_\perp^2}{3E_\perp} \int_0^\infty r^3 \exp(-2r) f_{\perp,1}(r) dr, \quad (18b)$$

The final task is to compute the radial parts $f_{\perp,l}(r)$ and $f_{\parallel,l}(r)$ of our function \mathbf{f} . We accomplish this by inserting the combination of Eqs (16a)-(16c) and (17a)-(17b) into Eq. (14). This procedure results in the following system of ordinary differential equations for the radial functions defined when $l > 0$ (see Appendix A for more details):

$$r^2 \hat{D}_r f_{\parallel,l} - l(l+1)f_{\parallel,l} = \lambda(\hat{\alpha}_l^0 f_{\parallel,l+2} + \hat{\beta}_l^0 f_{\parallel,l} + \hat{\gamma}_l^0 f_{\parallel,l-2}) - r^3 \delta_{l1}, \quad (19a)$$

$$r^2 \hat{D}_r f_{\perp,l} - l(l+1)f_{\perp,l} = \lambda(\hat{\alpha}_l^1 f_{\perp,l+2} + \hat{\beta}_l^1 f_{\perp,l} + \hat{\gamma}_l^1 f_{\perp,l-2}) - r^3 \delta_{l1}, \quad (19b)$$

where $\hat{\alpha}_l^m, \hat{\beta}_l^m, \hat{\gamma}_l^m$ are second order radial differential operators having the common structure

$$\hat{\alpha}_l^m = \alpha_{l,m}^{(0)} \left[r^2 \frac{\partial^2}{\partial r^2} + \left(\alpha_{l,m}^{(1)} - 2r \right) r \frac{\partial}{\partial r} + \alpha_{l,m}^{(2)} r + \alpha_{l,m}^{(3)} \right], \quad (20)$$

with different coefficients $\alpha_{l,m}^{(i)}, \beta_{l,m}^{(i)},$ and $\gamma_{l,m}^{(i)}$ as specified in Appendix A. Note that $\hat{\gamma}_1^0 = \hat{\gamma}_1^1 = 0$.

The solution to Eq. (19) with $\lambda = 0$ is known (see Appendix A). This suggests that a perturbative treatment of the differential problem is appropriate. With this in mind, we expand $f_{\perp,l}(r)$ and $f_{\parallel,l}(r)$ as power series in

$\lambda = 1 - \beta$. Letting $q = \{\parallel, \perp\}$, our radial functions take the form:

$$f_{q,l}(r) = f_{q,l}^{(0)}(r) + \lambda f_{q,l}^{(1)}(r) + \lambda^2 f_{q,l}^{(2)}(r) + \dots \quad (21)$$

Equating terms of like order in λ , we obtain a chain of differential equations for different $l \geq 1$ and $n \geq 0$:

$$r^2 \hat{D}_r f_{\parallel,l}^{(n)} - l(l+1)f_{\parallel,l}^{(n)} = (1 - \delta_{n0}) \left(\hat{\alpha}_l^0 f_{\parallel,l+2}^{(n-1)} + \hat{\beta}_l^0 f_{\parallel,l}^{(n-1)} + \hat{\gamma}_l^0 f_{\parallel,l-2}^{(n-1)} \right) - r^3 \delta_{l1} \delta_{n0} \quad (22a)$$

$$r^2 \hat{D}_r f_{\perp,l}^{(n)} - l(l+1)f_{\perp,l}^{(n)} = (1 - \delta_{n0}) \left(\hat{\alpha}_l^1 f_{\perp,l+2}^{(n-1)} + \hat{\beta}_l^1 f_{\perp,l}^{(n-1)} + \hat{\gamma}_l^1 f_{\perp,l-2}^{(n-1)} \right) - r^3 \delta_{l1} \delta_{n0} \quad (22b)$$

From this point forward, the solution method will be entirely iterative. Determination of $f_{q,l}^{(1)}$ requires $f_{q,l}^{(0)}$, $f_{q,l}^{(2)}$ requires $f_{q,l}^{(1)}$ and so forth. Note that Eqs. (22) with $n = 0$ reduce to Eqs. (19) with $\lambda = 0$. Since we know the solution for $\lambda = 0$ (see Appendix A), we use it as zeroth iteration, solve each differential equation for $f_{q,l}^{(1)}$ and proceed to the higher orders. The first few solutions are:

$$f_{\parallel,l}^{(0)} = f_{\perp,l}^{(0)} = \frac{r(r+2)}{4} \delta_{l1}, \quad (23a)$$

$$f_{\parallel,1}^{(1)} = \frac{r(r+3)}{5}, \quad (23b)$$

$$f_{\perp,1}^{(1)} = \frac{r(r-2)}{40}. \quad (23c)$$

The analytic form of the solutions past this point quickly becomes cumbersome. However, graphing the integrands $\lambda^n r^3 \exp(-2r) f_{q,1}^{(n)}(r)$ of the first three terms shows the rapid convergence of the series, as seen in Fig. 2.

The final expressions for the susceptibilities, utilizing

the expanded f ,

$$\chi_{\parallel} = \frac{8e^2 a_{\parallel}^2}{3E_{\perp}} (0.84375 + 0.8250\lambda + 0.8173\lambda^2 + \dots), \quad (24a)$$

$$\chi_{\perp} = \frac{8e^2 a_{\perp}^2}{3E_{\perp}} (0.84375 + 0.0094\lambda + 0.0058\lambda^2 + \dots), \quad (24b)$$

where for silicon $m_{\perp} = .191m_e$, $m_{\parallel} = .916m_e$, $a_{\perp} = 23.65 \text{ \AA}$, and $a_{\parallel} = 13.60 \text{ \AA}$. For these values of the effective masses and Bohr radii $E_{\perp} = 35.68 \text{ meV}$, $\lambda = 0.370$, and our susceptibilities are

$$\chi_{\parallel} \approx 1.74 \mu\text{eV}(\text{kV/cm})^{-2} \quad (25a)$$

$$\chi_{\perp} \approx 3.54 \mu\text{eV}(\text{kV/cm})^{-2}. \quad (25b)$$

III. VARIATIONAL METHOD

The findings of Section II provide very accurate asymptotic behavior of the energy levels at low electric fields. To achieve high accuracy for the Stark shifts of the ESR lines both at low and intermediate fields $\sim 5 \text{ kV/cm}$ we have to extend the scope of our methodology and use a specially crafted variational approach that is valid at higher fields and replicates the low-field results of the previous section.

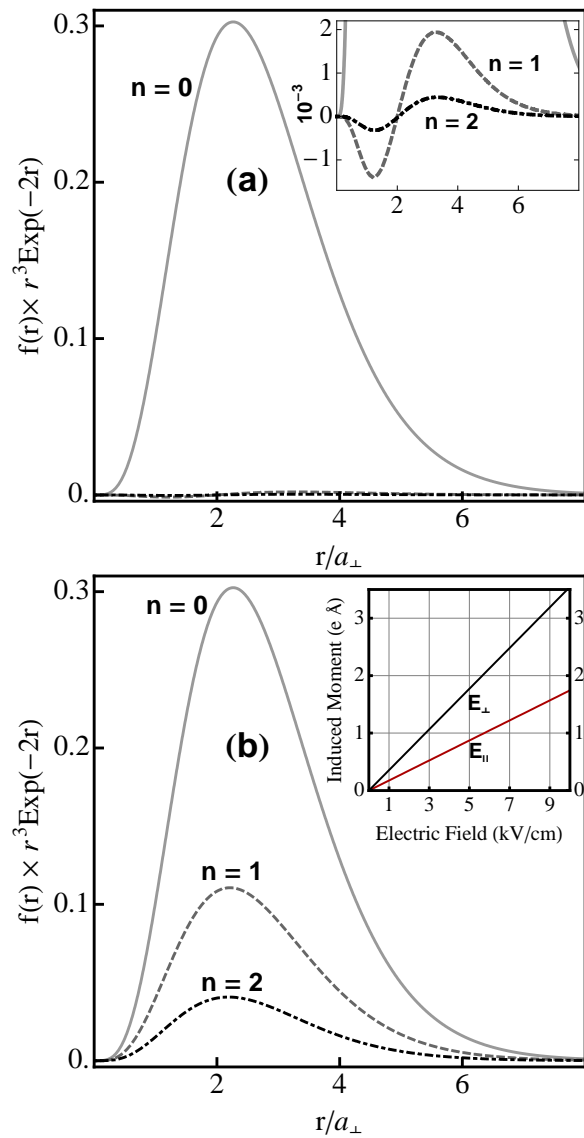


FIG. 2. (Color online.) The figures show successive integrands of (18) up to the second order term for fields lying in the x -direction (a) and the z -direction (b). The vertical axes are scaled appropriately for each graph, and the legend for both figures is shown in (b). The inset in (a) is a magnified view of the two dashed lines ($n = 1, 2$) that are not resolved in the main plot. The inset in (b) displays dipole moments induced by the electric fields parallel and perpendicular to the heavy-mass axis z .

Thus we seek to devise and use a trial function which will adequately represent the perturbed donor state, accurate up to at least the second order. This variational function will be used to extract expansions of the energy and the central cell electron density, which cannot be obtained from the second order perturbation theory. At low fields we will see converging results between the variational method of this section and the infinite-series perturbation theory of Section II.

In EMT, we can represent the orbital states of donors

in silicon with hydrogenic-like envelope functions. We expect that a homogeneous electric field will admix p -state components into this ground state. In hydrogen, each p -function with principle quantum number n will be of the form $rL_{n-2}^3(r/n) \exp(-2r/n)$ where L_{n-2}^3 is the generalized Laguerre polynomial of degree $n-2$. The higher p -states will contribute terms of order r^{n-1} to the perturbed state.

The higher p -states with principle quantum numbers $n \geq 3$ couple somewhat weaker to the ground state. However, since there are many of these states, it is reasonable to surmise that any highly accurate approximate method must account for their contributions. In summary, to accurately reflect the influence of the electric field on the hydrogenic wave functions of donors, our trial function must take into account the higher order radial contributions from the excited states.

It is instructive to illustrate our approach by considering the standard Hamiltonian for a hydrogen atom placed in a homogeneous electric field parallel to z -axis:

$$H = -\frac{\hbar^2}{2m_e} \nabla^2 - \frac{e^2}{r} - e\mathcal{E}z. \quad (26)$$

It can be shown that the exact first order expansion of the wave function, and the associated second order expansion of the ground state energy are^{32,33}

$$\psi(\mathbf{r}) = \psi_0(\mathbf{r}) + e\mathcal{E}f(\mathbf{r})\psi_0(\mathbf{r}), \quad (27)$$

$$E = -E_{Ry} - e^2\mathcal{E}^2 \langle \psi_0 | z f(\mathbf{r}) | \psi_0 \rangle, \quad (28)$$

where $f(\mathbf{r}) = (1/a_B E_{Ry})(r + 2a_B)z/4$ with a_B and E_{Ry} are the Bohr radius and the Rydberg energy respectively. The function $f(\mathbf{r}) = f_j(\mathbf{r})$ with $j = x, y, z$, is the isotropic analog of the function $\mathbf{f}(\mathbf{r})$ considered in the infinite-series summation of the previous section. The wave function (27) can be recast as

$$\psi(\mathbf{r}) = [1 + (q_1 + q_2 r)z] \exp(-r/a), \quad (29)$$

where $q_1 = e\mathcal{E}/2E_{Ry}$, $q_2 = e\mathcal{E}/4a_B E_{Ry}$, and $a = a_B$.

To extend our formalism to higher orders we can identify q_1 and q_2 as the first order expansion of some unknown *variational* parameters. Therefore we assume that the trial function takes the form of Eq. (29) with the unknown variational parameters $q_1 = q_1(\mathcal{E})$, $q_2 = q_2(\mathcal{E})$, and $a = a(\mathcal{E})$ to be determined via a standard minimization routine at an arbitrary field \mathcal{E} . This procedure leads to the following expansion of the energy expectation value:

$$\langle E \rangle = \frac{\langle \psi | H | \psi \rangle}{\langle \psi | \psi \rangle} = -E_{Ry} - \frac{9}{8} a_B^2 e^2 \mathcal{E}^2 / E_{Ry} + \dots, \quad (30)$$

which is in complete agreement with the exact second-order \mathcal{E} -field expansion of the ground state energy (28).

The term proportional to rz in Eq. (29) is responsible for admixture of the excited states into the ground state by the electric field. By including this term in the trial

function we were able to replicate the exact second order correction to the energy. In addition, the variational method allows for an efficient (albeit approximate) account of higher order terms outside of the perturbative regime. For the hydrogen atom, setting $q_2 = 0$ in Eq. (29) yields the following Taylor expansion of the expectation value of energy:

$$\langle E \rangle = -E_{Ry} - a_B^2 e^2 \mathcal{E}^2 / E_{Ry} + \dots \quad (31)$$

Thus by neglecting contributions of the excited states, we would introduce a relative error of 11% to the second order energy shift, running the risk of producing more significant errors in the higher orders.

In the case of the silicon donor states, our variational wave function must be generalized to reflect the anisotropy of the effective mass. To take this anisotropy into account, we will construct the trial function in the form similar to the hydrogenic function of Eq. (29), but with the appropriately scaled exponential and pre-exponential factors. Due to the axial symmetry of the Hamiltonian (5) at $\mathcal{E} = 0$ the \mathcal{E} -field vector can be chosen to lie in the (xz) -plane without any loss of generality. Thus our final variational function reads:

$$F_{+z}(\mathbf{r}) = F_z(\mathcal{E}) (1 + Q_{\perp}x + Q_{\parallel}z) \exp(-\varrho/a_{\perp}), \quad (32)$$

where $Q_{\perp} = q_{1\perp} + q_{2\perp}\varrho$, $Q_{\parallel} = q_{1\parallel} + q_{2\parallel}\varrho$, $\varrho = \sqrt{r^2 + (a_{\perp}^2/a_{\parallel}^2 - 1)z^2}$, and $F_z(\mathcal{E})$ is the normalization constant. Similar variational functions with normalization constants $F_j(\mathcal{E})$ can be defined for any valley s_j .

Friesen investigated the Stark effect for a phosphorous donors in silicon²⁰ using a single-valley variational method and a degenerate perturbation theory (see Eq. (38) below) to account for the valley-orbit effects. Our trial function (32) will reduce to that of Friesen's if we force parameters q_2 to zero, i.e. set and fix $q_{2\perp} = q_{2\parallel} = 0$. As we have seen from Eq. (31) it may lead to some inaccuracy in the low-field limit. In what follows we will use our improved single-valley variational function (32) and adopt Friesen's treatment of the valley-orbit effects. First, we compute the expectation energy of the single valley states, neglecting central cell contributions. For given γ and \mathcal{E} we take the expectation value of energy E_{s_j} to be a function of the parameters a_{η} , and the various $q_{1\eta}$ and $q_{2\eta}$ with $\eta = \{\parallel, \perp\}$. The energy

$$E_{s_j}(a_{\eta}, q_{1\eta}, q_{2\eta}; \gamma, \mathcal{E}) = \frac{\langle F_{s_j} | H_{s_j} | F_{s_j} \rangle}{\langle F_{s_j} | F_{s_j} \rangle}, \quad (33)$$

is minimized with respect to these parameters:

$$\frac{\partial E(\gamma, \mathcal{E})}{\partial a_{\eta}} = \frac{\partial E(\gamma, \mathcal{E})}{\partial q_{1\eta}} = \frac{\partial E(\gamma, \mathcal{E})}{\partial q_{2\eta}} = 0. \quad (34)$$

This condition implicitly defines the variational parameters as functions of the electric field. Using this knowledge, we can expand the single-valley ground state energy in Taylor series around zero field.

A simple system to test the variational function (32), is a hypothetical hydrogenic donor with the isotropic effective mass, $m_{\perp} = m_{\parallel}$, i.e. $\gamma = 1$. Since the unperturbed Hamiltonian displays spherical symmetry, we can take the z -axis to lie along the field direction. If we define our atomic units of energy and distance as $E_0 = \hbar^2/2m_{\perp}a_0^2$ and $a_0 = \hbar^2\kappa/2m_{\perp}e^2$, respectively, and minimize the energy according to (34) we obtain in the low-field limit: $q_{1\perp} = q_{2\perp} = 0$, $q_{1\parallel} = e\mathcal{E}/2E_0$, and $q_{2\parallel} = e\mathcal{E}/4a_0E_0$, in other words, we recover the exact expansions (29)-(30), where we replace $a_B \rightarrow a_0$ and $E_{Ry} \rightarrow E_0$. Similarly for the Friesen case with $q_{2\parallel} = 0$ we obtain a less accurate expansion (31), which does not comply with Rayleigh-Schrödinger perturbation theory.

It is expected that our variational function will return better corrections than previous methods, especially when used for small fields. For silicon, the effective mass anisotropy parameter $\gamma = 0.209$. We can no longer freely rotate the coordinate system due to a fixed heavy mass axis, and we will be required to keep track of the components of electric field parallel and perpendicular to this axis. Consider an envelope function of the valley s_j , $F_{s_j}(\mathbf{r}, \mathcal{E})$. To study the valley-orbit corrections due to the central cell contact potential we will need the values of $F_{s_j}(0, \mathcal{E}) \equiv F_j(\mathcal{E})$ at $\mathbf{r} = 0$. Our computations proceed as in the isotropic hydrogenic case, and we obtain the second-order expansion of the energy and the central cell amplitudes:

$$E = E_0 - \frac{1}{2}\chi_{\parallel}\mathcal{E}_{\parallel}^2 - \frac{1}{2}\chi_{\perp}\mathcal{E}_{\perp}^2, \quad (35a)$$

$$F_j(\mathcal{E})/F_0 = 1 - \frac{1}{2}f_{\parallel}^{(2)}\mathcal{E}_{\parallel}^2 - \frac{1}{2}f_{\perp}^{(2)}\mathcal{E}_{\perp}^2. \quad (35b)$$

Here, \mathcal{E}_{\parallel} and \mathcal{E}_{\perp} are the field components parallel and perpendicular to the heavy-mass axis of the valley s_j , $F_0 = F_j(0)$ is the normalization constant at zero field, and the numerical values of the susceptibilities and coefficients $f^{(2)}$ are:

$$\chi_{\parallel} = 1.71 \mu\text{eV}(\text{kV}/\text{cm})^{-2}, \quad (36a)$$

$$\chi_{\perp} = 3.63 \mu\text{eV}(\text{kV}/\text{cm})^{-2}, \quad (36b)$$

$$f_{\parallel}^{(2)} = 1.53 \times 10^{-4} (\text{kV}/\text{cm})^{-2}, \quad (36c)$$

$$f_{\perp}^{(2)} = 2.82 \times 10^{-4} (\text{kV}/\text{cm})^{-2}. \quad (36d)$$

We see good agreement with the susceptibilities presented in Eqs. (25a) and (25b). Additionally, we can check the answers obtained using Friesen's previous results. As before, by setting $q_{2\perp}$ and $q_{2\parallel}$ to zero and holding them fixed, we obtain equivalent results for Friesen's variational function:

$$\chi_{\parallel} = 1.58 \mu\text{eV}(\text{kV}/\text{cm})^{-2}, \quad (37a)$$

$$\chi_{\perp} = 3.17 \mu\text{eV}(\text{kV}/\text{cm})^{-2}, \quad (37b)$$

$$f_{\parallel}^{(2)} = 1.54 \times 10^{-4} (\text{kV}/\text{cm})^{-2}, \quad (37c)$$

$$f_{\perp}^{(2)} = 2.69 \times 10^{-4} (\text{kV}/\text{cm})^{-2}, \quad (37d)$$

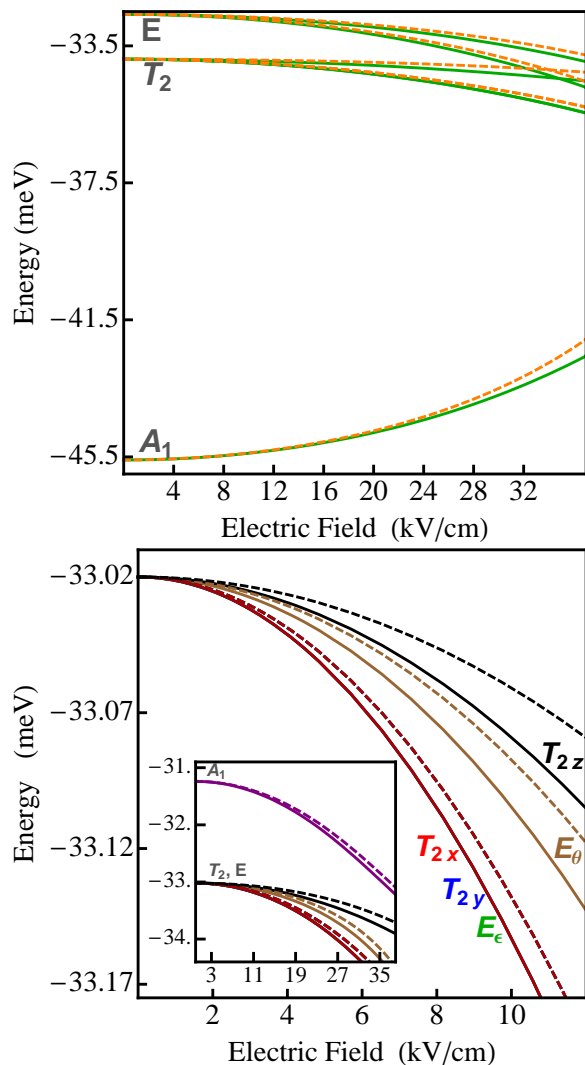


FIG. 3. (Color online.) The plot on the top shows the comparison between our results (solid lines) and Friesen's (dashed) for the spectrum of a phosphorous donor in silicon. The second plot shows the spectrum of a lithium donor, where the dashed lines correspond to Friesen's variational function ($q_{2\perp} = q_{2\parallel} = 0$) for Li.

With the variational functions at hand we can construct the valley-orbit Hamiltonian^{20,37} in the presence of the electric field:

$$H_{vo}(\mathcal{E}) = \sum_{s,i} (E_{0i} + \Delta_{0i}) |si\rangle \langle si| + \sum_{i,s} \Delta_{1i} |si\rangle \langle -si| + \sum_{i,j,s,s'} \Delta_{2ij} (1 - \delta_{ij}) |si\rangle \langle s'j|, \quad (38)$$

where E_{0i} may be written as $E_{0i} = E_0 - \frac{1}{2}\chi_{\perp}\mathcal{E}^2 + \frac{1}{2}(\chi_{\perp} - \chi_{\parallel})\mathcal{E}_i^2 + \dots$. Other corrections to the terms involving E_{0i} will be left to the next section. The matrix elements Δ_q of the central cell contact potential between the valley-orbitals (3) describe the central cell shift (Δ_0) and the valley-orbit splittings (Δ_1 and Δ_2) of the energy

levels. Following Friesen's prescription,²⁰ we parametrize the matrix elements Δ_q as follows:

$$\Delta_{0j} = \nu_0 F_j^2(\mathcal{E}), \quad (39a)$$

$$\Delta_{1j} = \nu_1 F_j^2(\mathcal{E}), \quad (39b)$$

$$\Delta_{2ij} = \nu_2 F_i(\mathcal{E}) F_j(\mathcal{E}). \quad (39c)$$

The parametrization in Eqs. (39a)-(39c) assumes that the central cell potential has a contact (i.e. δ -function like) form. The fitting parameters ν_k depend on the choice of the variational functions to ensure that the experimental spectrum at zero field is reproduced correctly. For our variational functions defined by Eq. (32), it gives the following values of the parameters ν_i in Si:Li: $\nu_0 = -34.54 \text{ eV}\cdot\text{\AA}^3$, $\nu_1 = 7.09 \text{ eV}\cdot\text{\AA}^3$, and $\nu_2 = 7.09 \text{ eV}\cdot\text{\AA}^3$. In Fig. 3, we compare the spectra of P and Li shallow donors calculated with ours and Friesen's variational functions for an external electric field in 001 direction. For phosphorous impurity our approach does not produce substantial differences at low and intermediate fields. For lithium, on the other hand, the effect is more significant due to the nearly degenerate ground state.

At this juncture, we need to consider the two competing effects caused by the electric field. The first effect is the direct quadratic Stark shift of the single-valley Coulomb binding energies E_{0i} . This effect will be similar to that of strain upon the donor spectrum, as we discuss below in section IV. The second effect is based on the fact that by pulling the lithium donor electron away from the central cell, the electric field reduces the magnitude of the matrix elements Δ_q . This will bring the levels closer to their "center of gravity" and narrow the overall energy spectrum of the $1s$ manifold.²⁰ For Li donors subject to relatively low electric fields below ionization threshold, this *spectrum narrowing* effect may be treated separately and independently from the Stark shift of the valley energies E_{0i} by means of the second-order expansion of the variational parameters, as detailed in Section V and Appendix B.

IV. EFFECT OF STRAIN AND ELECTRIC FIELD

We wish to consider the interplay of the Stark effect with the effects due to other influences such as strain and magnetic field. Both the electric field and strain in the silicon lattice will cause a change of the six single-valley energies that emerge on the diagonal of the valley-orbit Hamiltonian (38). By virtue of the ellipsoidal valley symmetry these energies will not depend on index s and for a given valley si , we can write both the quadratic Stark effect and the strain corrections to the energy as $E_{si} = E_{0i} = E_0 - \delta_i(\mathcal{E}) - \delta_i(e_{jk})$ such that

$$\delta_i(\mathcal{E}) = -\frac{1}{2}\chi_{\perp}\mathcal{E}^2 + \frac{1}{2}(\chi_{\perp} - \chi_{\parallel})\mathcal{E}_i^2, \quad (40a)$$

$$\delta_i(e_{jk}) = \Xi_d(e_{xx} + e_{yy} + e_{zz}) + \Xi_u e_{ii}, \quad (40b)$$

where e_{jk} are the components of the strain tensor at the donor location and Ξ_d and Ξ_u are the dilation and shear deformation-potential constants of Si conduction band minimum.³⁸ The nearly degenerate ground state manifold of the Li donor is very sensitive to strain. However a simple dilation merely shifts the levels by the same amount, $\Delta E = (\Xi_d + \Xi_u/3)(e_{xx} + e_{yy} + e_{zz})$, and does not alter their separation. To change the relative positions of the energy levels and lift the fivefold degeneracy of the ground state, at least one of the two linear combinations of the strain tensor components

$$e_\theta = e_{zz} - \frac{1}{2}(e_{xx} + e_{yy}), \quad e_\epsilon = \frac{\sqrt{3}}{2}(e_{xx} - e_{yy}) \quad (41)$$

must be different from zero.³

In a similarity, a uniform electric field can also lift the degeneracy. The quadratic Stark effect can be described by the variables

$$w_\theta = \frac{1}{2}(3n_z^2 - 1), \quad w_\epsilon = \frac{\sqrt{3}}{2}(n_x^2 - n_y^2), \quad (42)$$

where $n_{x,y,z}$ are components of the unit vector \mathbf{n} in the direction of the electric field

$$\mathcal{E} = \mathcal{E} \mathbf{n}, \quad \mathbf{n} = (n_x, n_y, n_z). \quad (43)$$

Therefor to account for the strain effects, we must add the strain energies (40b) to the diagonal of the valley-orbit matrix (see Eq. (38)) in $|si\rangle$ basis. To the second order in \mathcal{E} , we may combine the strain and Stark terms and separate them from the zero field valley-orbit Hamiltonian (2). Fixing the average energy of the $1s$ manifold at zero, the combined Hamiltonian, describing strain and electric field effects, may be written as

$$\hat{H}_S = \Xi_u \left(v_\theta \hat{V}_\theta + v_\epsilon \hat{V}_\epsilon \right), \quad (44)$$

where $\Xi_u = 11.4$ eV. Here \hat{V}_θ and \hat{V}_ϵ are operators in the space spanned by the six symmetrized orbitals $|\mu\rangle$

$$\begin{aligned} \hat{V}_\theta = & \frac{1}{3} (|E_\theta\rangle\langle E_\theta| - |E_\epsilon\rangle\langle E_\epsilon| - |T_{2x}\rangle\langle T_{2x}| - |T_{2y}\rangle\langle T_{2y}|) \\ & + \frac{2}{3} |T_{2z}\rangle\langle T_{2z}| + \frac{\sqrt{2}}{3} (|A_1\rangle\langle E_\theta| + |E_\theta\rangle\langle A_1|), \end{aligned} \quad (45a)$$

$$\begin{aligned} \hat{V}_\epsilon = & \frac{1}{\sqrt{3}} (|T_{2x}\rangle\langle T_{2x}| - |T_{2y}\rangle\langle T_{2y}|) \\ & + \frac{1}{3} \left(\sqrt{2} |A_1\rangle\langle E_\epsilon| - |E_\theta\rangle\langle E_\epsilon| + H.C. \right), \end{aligned} \quad (45b)$$

where $H.C.$ denotes hermitian conjugation.

In Eq. (44), the variables v_θ and v_ϵ are linear combinations of terms describing the effects of strain and electric field:

$$v_\theta = e_\theta + \kappa \mathcal{E}^2 w_\theta, \quad (46a)$$

$$v_\epsilon = e_\epsilon + \kappa \mathcal{E}^2 w_\epsilon, \quad (46b)$$

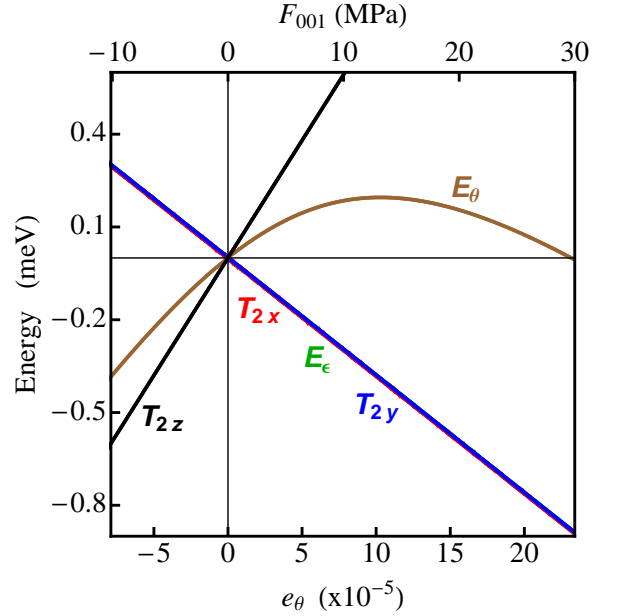


FIG. 4. (Color online.) Dependence of the 5 lowest orbital energy levels of Si:Li donor electron on the uniaxial [001] strain. Dominant characters of the states are given with letters. Color of the lines also encodes the dominant characters of the states for each value of e_θ .

where

$$\kappa = \frac{1}{2} \frac{\chi}{\Xi_u} \approx 10^{-7} \left(\frac{\text{kV}}{\text{cm}} \right)^{-2}, \quad (47)$$

and $\chi = \chi_\perp - \chi_\parallel = 1.9 \mu\text{eV}(\text{kV}/\text{cm})^{-2}$ is the anisotropic part of the quadratic Stark effect susceptibility. The quantities v_ϵ and v_θ in Eqs. (46) can be viewed as “effective strain” variables. The quadratic Stark effect due to the field $1 \text{ kV}/\text{cm}$ is equivalent to a very small strain $\sim 10^{-7}$. Larger electric fields of the order of $3 \text{ kV}/\text{cm}$ will be equivalent to the strain $\sim 10^{-6}$.

Elaborating on the analogy between strain and electric field, the two effective strain parameters determine the orbital response when actual strain or electric fields are present. For simplicity, let us initially consider the case when $v_\epsilon = 0$ but v_θ is nonzero. As follows from Eqs. (41), (42), (46a) and (46b), the degeneracy of the Li ground state quintet can be partially lifted either with uniaxial strain along [100], or with biaxial isotropic strain in the (xy) -plane, or with some combination thereof. The states T_{2x} , T_{2y} and E_ϵ , which do not contain any contribution from $|\pm z\rangle$, valley-orbitals will remain degenerate. The nature of the strain determines the structure of the ground state. A tensile uniaxial strain along [001] has $v_\theta > 0$ and favors the $(T_{2x}, T_{2y}, E_\epsilon)$ triplet ground state. Contrariwise, the non-degenerate ground state T_{2z} and the first excited state E_θ correspond to a compressive uniaxial [001] strain with $v_\theta < 0$. These findings are summarized in Fig. 4.

One can relate the effective strains produced by an imposed external stress using the three-dimensional Hooke’s

law for an isotropic material: $e_\theta = (1 + \nu)(\sigma_{zz} - \frac{1}{2}(\sigma_{xx} + \sigma_{yy}))/E$ and $e_\epsilon = \frac{\sqrt{3}}{2}(1 + \nu)(\sigma_{xx} - \sigma_{yy})/E$. Here, E and ν are the Young's modulus and Poisson's ratio, respectively, and σ_{jj} is the applied stress component along the j th axis. If we wish to create a condition with $e_\theta \neq 0$ and $e_\epsilon = 0$, we require $\sigma_{xx} = \sigma_{yy}$ and find $e_\theta = (1 + \nu)(\sigma_{zz} - \sigma_{xx})/E$. In short, to prepare a three-fold degenerate ground state $(T_{2x}, T_{2y}, E_\epsilon)$, a uniaxial tension along [001] is sufficient. As we will see below, an additional stress along [100] or [010] will result in $v_\epsilon \neq 0$ and completely lift the orbital degeneracy.

We can create similar conditions with the electric field. To keep $v_\epsilon = 0$ at nonzero field, the electric field must be confined to the plane formed by the [001] axis and either the [110] or the $[1\bar{1}0]$ axes. The uniaxial strain can be replicated by electric fields lying in this plane. An electric field parallel to [001] replicates tensile uniaxial strain, while fields parallel to either [110] or $[1\bar{1}0]$ replicate compressive uniaxial strain. Pointing the electric field away from these axes, but still within the plane in question, only results in reducing the effective strain v_ϵ , which vanishes entirely for a field parallel to [111].

One can expect a non-trivial interplay of the Zeeman and Stark effects due to multiple level crossings in the ground state manifold. The possibility of the ground state Stark splitting makes the Li impurity unique among other shallow donors in Si and opens exciting opportunities for electrical manipulation of the spin qubits. As we will show below, the values of the electric field in 1-3 kV/cm range are sufficient to produce large changes in g -factors near the points of avoided crossing between the donor electron energy levels controlled by Zeeman and spin-orbit interaction.

To examine this interplay further, we want to introduce a second source of effective strain v_ϵ , in this case such that $|v_\theta| \gg |v_\epsilon| > 0$. A nonzero strain v_ϵ separates the triplet manifold $(T_{2x}, T_{2y}, E_\epsilon)$, allowing us to maximize the spin-orbit effects and control g -factors. A biaxial strain anisotropy or an electric field lying in the (xy) -plane will produce nonzero v_ϵ . In general, we should note that the increase of strain or electric field along a single crystallographic axis will change the value of v_θ by $v_\epsilon\sqrt{3}/3$. For our purposes, we consider $v_\theta \approx 10^{-4}$, which will not be seriously influenced by $v_\epsilon \approx 10^{-6}$. As long as $|v_\epsilon| \ll |v_\theta|$, the correction to v_θ will not introduce any serious errors to the spin-orbit interactions within the ground state triplet $(T_{2x}, T_{2y}, E_\epsilon)$.

As before, we can think of the electric field as analogous to strain. In general, electric fields lying in the (xy) -plane will produce a nonzero effective strain v_ϵ . The influence of the electric field on v_ϵ is maximal along the crystallographic axes and vanishes entirely along [110] or $[1\bar{1}0]$. The field along [100] produces "tensile" effective strain $v_\epsilon > 0$ while the field along [010] produces a "compressive" effective strain $v_\epsilon < 0$.

Despite having similar qualitative features, the electric field effects are considerably weaker than those of strain. Additionally, strong electric fields will ionize the Li donor

and may even induce electrical breakdown within the silicon. For this reason we will consider only moderate electric fields in 1-3 kV/cm range and envision their role as a means of precise fine tuning and control of the Li donor spectrum. We must rely on tensile strain e_θ to split the Li quintet and isolate the $(T_{2x}, T_{2y}, E_\epsilon)$ ground state triplet. The fine tuning by the electric field will then induce much smaller effective strain v_ϵ . By inducing the splitting of the $(T_{2x}, T_{2y}, E_\epsilon)$ triplet, the electric field can be used to explore the effects of the spin-orbit interaction through g -factor control of ESR spectra.

V. EFFECT OF SPECTRUM NARROWING

Electric fields can influence the donor spectrum in a strain-like way, however, higher-order confounding effects emerge through the electric field dependence of the valley-orbit matrix elements Δ_{0j} , Δ_{1j} , and Δ_{2ij} . Generally speaking, these spectrum narrowing effects violate relationship between strain and electric field. However, the analogy described in Sec. IV, remains intact if we are only concerned with the influence of the electric field upon the isolated $(T_{2x}, T_{2y}, E_\epsilon)$ manifold.

Appendix B details a procedure for constructing the orbital Hamiltonian with strain, electric field and spectral narrowing effects taken. Let us consider a truncated version of the Hamiltonian given in Eq. (B8) restricted to the $\{|E_\epsilon\rangle, |T_{2x}\rangle, |T_{2y}\rangle\}$ Hilbert subspace. We assume that a uniaxial tensile stress has separated the other levels and isolated the ground state triplet manifold. Then, as described in appendix B, the spectrum narrowing Hamiltonian will have the form

$$\hat{H}_{sn} = (q_\theta + q_\eta) (|E_\epsilon\rangle \langle E_\epsilon| + |T_{2x}\rangle \langle T_{2x}| + |T_{2y}\rangle \langle T_{2y}|) + \frac{q_\epsilon}{\sqrt{3}} (|T_{2x}\rangle \langle T_{2x}| - |T_{2y}\rangle \langle T_{2y}|). \quad (48)$$

The form of each q will be

$$q_\theta = -\frac{1}{3}F_0^2\nu_0 \left(f_\perp^{(2)} - f_\parallel^{(2)} \right) \mathcal{E}^2 w_\theta, \quad (49a)$$

$$q_\epsilon = \frac{1}{2} \left[2F_0^2(\nu_0 - \nu_1) \left(f_\perp^{(2)} - f_\parallel^{(2)} \right) \right] \mathcal{E}^2 w_\epsilon, \quad (49b)$$

$$q_\eta = \frac{1}{2}F_0^2\nu_1 \left(f_\perp^{(2)} + f_\parallel^{(2)} + \left(f_\perp^{(2)} - f_\parallel^{(2)} \right) n_z^2 \right) \mathcal{E}^2, \quad (49c)$$

where the parameters ν_k , $f^{(2)}$ and F_0 are defined in Section III.

Because the ground state triplet manifold is well separated from the rest of the states with higher energy their contribution to the triplet level shifts is negligible. As previously, we eliminate the terms shifting the triplet levels by an equal amount and set the energy origin at the "center of gravity" of the triplet manifold. Then the primary effect of spectrum narrowing will consist in renormalization of the Stark susceptibility. At the same time, the analogy between electric field and strain remains intact within the ground state (i.e. triplet) manifold. The

new effective strain variable controlling the splitting of the triplet levels can be written as

$$v_\epsilon = e_\epsilon + \frac{1}{2} \frac{\chi'}{\Xi_u} \mathcal{E}^2 w_\epsilon \quad (50)$$

where χ' is the effective susceptibility given by

$$\begin{aligned} \chi' &= \chi + 2F_0^2 (\nu_0 - \nu_1) (f_\perp^{(2)} - f_\parallel^{(2)}) \\ &\approx 1.5 \mu\text{eV}(\text{kV}/\text{cm})^{-2}. \end{aligned} \quad (51)$$

While this susceptibility is slightly reduced, we demonstrate that it is still large enough to induce dramatic shifts of electron g -factors as well as overall reshaping of ESR lines.

VI. EFFECTS OF ZEEMAN AND SPIN-ORBIT INTERACTIONS

The full donor electron Hamiltonian,

$$\hat{H} = \hat{H}_{vo}(\mathcal{E}, e_{ij}) + \hat{H}_Z + \hat{H}_{so}, \quad (52)$$

includes the valley-orbit, strain and Stark effects as well as the spin-Zeeman and spin-orbit interactions³ characterized by g -factor anisotropy and by two spin-orbit constants³

$$g_\perp = 1.9984, \quad g_\parallel = 1.9994, \quad (53)$$

$$\lambda_1 = 2.6 \mu\text{eV}, \quad \lambda_2 = 6.9 \mu\text{eV}. \quad (54)$$

We can recast the spin-orbit Hamiltonian using vector operators similar to those introduced by Watkins and Ham³:

$$H_{so} = \frac{1}{2} (\lambda_1 \hat{\mathbf{L}}_1 + \lambda_2 \hat{\mathbf{L}}_2) \cdot \hat{\boldsymbol{\sigma}}, \quad (55)$$

where

$$\hat{\mathbf{L}}_1 = -\frac{i}{2} \sum_{ij} \sum_{ss'} |si\rangle s [\mathbf{n}_i \times \mathbf{n}_j] s' \langle s'j|, \quad (56)$$

$$\hat{\mathbf{L}}_2 = -\frac{1}{2\sqrt{2}} \sum_{ij} \sum_{ss'} |si\rangle ([\mathbf{n}_i \times \mathbf{n}_j] \cdot \boldsymbol{\tau}) (\mathbf{n}_i s - \mathbf{n}_j s') \langle s'j|, \quad (57)$$

where $\boldsymbol{\tau} = (1, 1, 1)$, $\hat{\boldsymbol{\sigma}} = (\hat{\sigma}_x, \hat{\sigma}_y, \hat{\sigma}_z)$, and $\hat{\sigma}_i$ are the conventional Pauli matrices. Similarly, the Zeeman Hamiltonian can be expressed as:

$$H_Z = \frac{1}{2} g_\perp \mu_B \left[\hat{\boldsymbol{\sigma}} \cdot \mathbf{B} + \varepsilon \sum_{is} |is\rangle \hat{\sigma}_i B_i \langle is| \right], \quad (58)$$

where $\varepsilon = (g_\parallel - g_\perp)/g_\perp = 5 \times 10^{-4}$.

In ESR studies, pulses of ac magnetic field excite donor electron spins coupled via the magnetic dipole interaction to a cavity mode with fixed frequency ω_0 . By varying

the strength of the external static magnetic field \mathbf{B} , the cavity mode is excited every time when the resonance condition, $E_n - E_m = \hbar\omega_0$, is fulfilled. Here $E_n - E_m$ is a Zeeman splitting for the transition between states with predominantly opposite spin orientations. The spin-orbit interaction³ gives rise to shifts $\hbar\Delta_{nm}$ of the Zeeman splitting for spin-flip transitions

$$E_n - E_m = g_\perp \mu_B B + \hbar\Delta_{nm}. \quad (59)$$

Each transition corresponds to a specific value of static magnetic field B_{nm} at which the resonance with cavity mode is achieved. It is customary to formally introduce g -factors instead of B_{nm} for each transition

$$g_{nm} = \frac{\hbar\omega_0}{\mu_B B_{nm}}, \quad E_n - E_m = \hbar\omega_0, \quad (60)$$

where μ_B is Bohr magneton. In general, the Zeeman shift Δ_{nm} is a function of magnetic field magnitude (B) and orientation ($\boldsymbol{\tau}$) as well as of the value of the effective strain (v_ϵ) at the donor location. Introducing a cyclotron frequency, $\omega = \frac{1}{\hbar} g_\perp \mu_B B$, the values of g -factors g_{nm} at each resonance equal

$$g_{nm} = g_\perp \frac{\omega_0}{\omega_{nm}}, \quad (61)$$

where $\omega = \omega_{nm}$ is a root of algebraic equation (cf. (59))

$$\omega = \omega_0 - \Delta_{nm}(\omega, \boldsymbol{\tau}, v_\epsilon). \quad (62)$$

It is of interest to study the g -factor for each transition as function of magnetic field orientation and effective strain:

$$g_{nm} = g_\perp \frac{1}{1 - \frac{1}{\omega_0} \Delta_{nm}(\omega_{nm}, \boldsymbol{\tau}, v_\epsilon)}. \quad (63)$$

Assuming that the bare Zeeman energy is much greater than the spin-orbit interaction, $\hbar\omega \gg \lambda_1, \lambda_2$, the corresponding shifts in Zeeman splitting $\Delta_{nm}(\omega)$ for each transition can be found from the successive orders of perturbation theory corrections to the energy levels E_n . As a result, each shift Δ_{nm} can be obtained in a form of an expansion in inverse powers of ω :

$$\Delta_{nm} = d_0^{nm} + d_1^{nm} \omega^{-1} + d_2^{nm} \omega^{-2} + d_3^{nm} \omega^{-3} + \dots \quad (64)$$

Because the energy corrections contain the powers of bare Zeeman splittings in the denominator, the expansion (64) does not have positive powers of ω . The term with zero power of ω in (64) occurs when states with the same energy have very close energies and coupled by spin-orbit interaction. The latter then splits the Zeeman transition frequencies already in zeroth order in $\lambda_{1,2}$ (this happens in our case as will see below). Plugging (64) into (62) and inverting the series expansion, one can find a root of (62) for a given transition, $\omega = \omega_{nm}$, in terms of inverse powers of ω_0 . Then, expressing magnetic field B_{nm} in (60) via ω_{nm} gives the g -factor in the form

$$g = g_\perp \left(1 + \frac{d_0}{\omega_0} + \frac{d_0^2 + d_1}{\omega_0^2} + \frac{d_0^3 + 3d_0 d_1 + d_2}{\omega_0^3} + \dots \right), \quad (65)$$

where we omitted the state indexes for simplicity. In general, for a given Li donor the g -factors for individual transitions depend on both the electric field and the strain at the donor location through the effective strain variables v_θ , v_ϵ , as well as on the magnetic field orientation.

Typically, g -factor shifts are very small in the $1s(A_1)$ ground state of substitutional shallow donors in silicon because the spin-orbit interaction only involves excited states $1s(E+T_2)$ and the corresponding corrections contain very large energy denominators for the valley-orbit splitting between the singlet and the rest of $1s$ levels. In the Li donor, the situation is different because the bundle of levels, $1s(E+T_2)$, with little or no valley-orbit splitting is now a ground state. It is exactly the zero- th order term $\propto d_0$ in Eq. (64), resulting from this degeneracy, that gives rise to very large g -factor shifts. Below we will analyze various types of the spin-flip transitions in the vicinity of the avoided crossing. At the avoided crossing the situation is quite involved because the spin-orbit coupling mixes the states with different orbital characters. The role of (xy) -plane strain or electric field is to lift the level degeneracy and to promote direct spin-flip transitions between the states with the same orbital characters.

VII. G-FACTOR CONTROL WITH ELECTRIC FIELDS

Here we consider a uniaxial tensile stress along $[001]$ amended by an electric field along $[100]$. This combination of stress and electric field leads to effective strains v_θ , v_ϵ such that $|v_\theta| \gg |v_\epsilon|$. The small, yet nonzero, effective strain v_ϵ splits the triplet levels according to Eq. (45b). If we include the electron spin in the triplet, we have a sextet of spin-orbital electron states. For uniaxial tensile stress $\sigma_{001} \approx 30$ MPa and magnetic field 0.343 T (corresponding to an ESR cavity mode of frequency $\omega_0 = 9600$ MHz), the energy gap separating a ground state spin-orbit sextet from the higher-lying states is of the order of 1 meV (cf. Fig. 4), and it is much greater than the Zeeman splittings within the sextet ($\sim 40 \mu\text{eV}$). Therefore, for sub-Kelvin temperatures, the system can be described by a reduced Hamiltonian operating on the sextet of electron spin states. In what follows, we shall study the effects of spin-orbit interaction, small v_ϵ , and magnetic fields upon this sextet.

The dependence of the lower triplet of energy levels on the effective strain variable v_ϵ is shown in Fig. 5 for the case of a magnetic field in $[001]$ direction. The level structure is symmetric with respect to $\pm v_\epsilon$. The behavior of these levels can be understood from the fact that when stress and magnetic field are aligned with the same crystal axis (z) the eigenstates of the donor electron Hamiltonian split into two subspaces. The first subspace is formed by the states $|E_\epsilon, \frac{1}{2}\rangle$, $|T_{2x}, -\frac{1}{2}\rangle$, $|T_{2y}, -\frac{1}{2}\rangle$ while the other one corresponds to the opposite spin projections on magnetic field direction. The states $|\Phi_\pm\rangle$ belong-

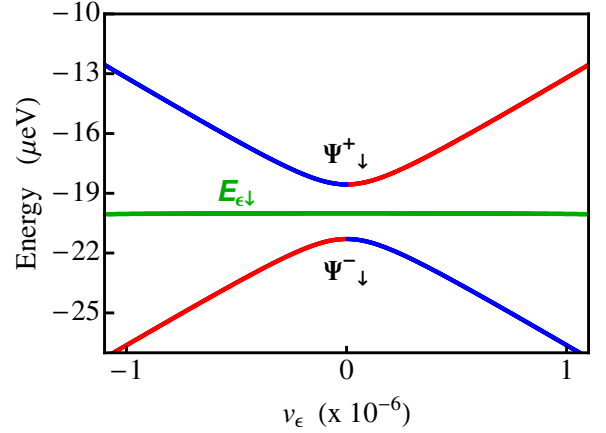


FIG. 5. (Color online.) Plot shows the level diagram in the vicinity of one of the avoided crossing at $v_\epsilon=0$. Blue, green and red line colors correspond to the dominant orbital characters T_{2y} , E_ϵ , and T_{2x} , respectively. Symbols Ψ_\downarrow^\pm indicate the eigenstates (70) for the corresponding energy levels.

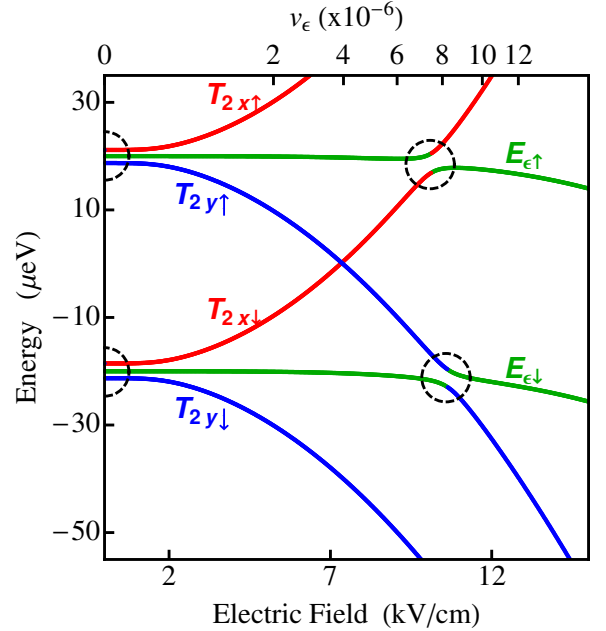


FIG. 6. (Color online.) Plot shows dependence of the six lowest energy levels on $[100]$ electric field with uniaxial tension $\sigma_{001} = 30$ MPa and magnetic field $B_{001} = 0.343$ T.

ing to different subspaces are eigenstates of the operator $\hat{Z} = \hat{R}_z(\pi)\hat{\sigma}_z$, which commutes with the Hamiltonian. Here $\hat{R}_z(\pi)$ is the operator of rotation through angle π about the z -axis and $\hat{Z}|\Phi_\pm\rangle = \pm|\Phi_\pm\rangle$. Due to this symmetry, the eigenvalues of \hat{Z} are good quantum numbers and the spin-orbit interaction couples the states within each subspace, but not between the subspaces.

For the eigenstates of the donor Hamiltonian, neither the orbital characters ($T_{2x}, T_{2y}, E_\epsilon$) nor the spin projections (\uparrow, \downarrow) are good quantum numbers. Nonetheless, we

will label these eigenstates as $T_{2x\uparrow}$, $E_{\epsilon\downarrow}$ etc., keeping in mind that this is *predominant*, albeit approximate, character of a given eigenstate.

As shown in Fig. 6, when a [100] electric field increases from zero, the levels T_{2x} and T_{2y} are shifted quadratically with the field (linearly with v_ϵ) in opposite directions while the level E_ϵ does not change in the first order in v_ϵ (its variation occurs in the second order from coupling to higher lying states E_θ , A_1 as $\Delta E = -\eta_\epsilon v_\epsilon^2$ with $\eta_\epsilon = 45$ keV). For a given magnetic field and effective strain $v_\epsilon = \bar{v}_\epsilon$ such that

$$\frac{\Xi_u}{\sqrt{3}}\bar{v}_\epsilon - \eta_\epsilon \bar{v}_\epsilon^2 = \hbar\omega, \quad (66)$$

($\bar{v}_\epsilon \approx 6.3 \times 10^{-6}$ for $B_{001} = 0.343$ T), there exists an avoided crossing between the levels corresponding to the states with dominant characters $|T_{2y}, \frac{1}{2}\rangle$ and $|E_\epsilon, -\frac{1}{2}\rangle$. Higher in energy by approximately $g\mu_B B$ there exists another avoided crossing between $|E_\epsilon, \frac{1}{2}\rangle$ and $|T_{2x}, -\frac{1}{2}\rangle$ ($\mathcal{E} \simeq 11$ kV/cm in Fig. 6). For $v_\epsilon \approx -\bar{v}_\epsilon(\omega)$, there exists a similar pair of avoided crossings where the orbital character T_{2x} is replaced by T_{2y} and vice versa. We note that for the twice smaller value of $v_\epsilon \approx 3 \times 10^{-6}$ ($\mathcal{E} \simeq 8$ kV/cm), the energy levels of the states $|T_{2x}, -\frac{1}{2}\rangle$, $|T_{2y}, \frac{1}{2}\rangle$ undergo a real crossing because these states are not coupled to each other by the spin-orbit interaction.

A different type of avoided-crossing exists for $v_\epsilon \approx 0$. It occurs between the levels corresponding to the states with the same spin orientation and predominant orbital characters $|T_{2x}\rangle$ and $|T_{2y}\rangle$. We note the energies of the states T_{2x} , T_{2y} , and E_ϵ with the same spin projection are very close to each other. Despite this, the state E_ϵ is not coupled to the other two by the spin-orbit interaction. Therefore energy levels of the states with dominant characters $|E_\epsilon, \pm\frac{1}{2}\rangle$ are only weakly perturbed by spin-orbit interaction and effective strain v_ϵ (see above).

The level splitting for the the avoided crossing between states with opposite spin orientations, λ_2 , is about twice larger than that between the states with the same spin orientation (corresponding to λ_1). However, in either case the, level repulsion at the avoided crossings is much smaller than the Zeeman energy, and therefore, the analysis of the avoided crossings can be done to a leading order within the two-state approximation. In what follows, we will use the two-state approximation and consider the effects of the spin-orbit interactions near the avoided crossings at $v_\epsilon = 0$ and $v_\epsilon \approx 6.3 \times 10^{-6}$.

We consider truncated Hamiltonians to describe the avoided-crossings at $v_\epsilon=0$. As E_ϵ is not coupled by the spin-orbit interaction to the other states, a two-level Hamiltonian in the basis of the corresponding pairs of states $|T_{2x}, \frac{1}{2}\rangle$, $|T_{2y}, \frac{1}{2}\rangle$ and $|T_{2x}, -\frac{1}{2}\rangle$, $|T_{2y}, -\frac{1}{2}\rangle$ is appropriate. The form of these Hamiltonians can be written as

$$\Delta H_{\pm 1/2}^{\text{ac}} = \pm \frac{\hbar\omega}{2} \begin{pmatrix} 1 & 0 \\ 0 & 1 \end{pmatrix} - \frac{\lambda_1}{2} \begin{pmatrix} w & \pm i \\ \mp i & -w \end{pmatrix}, \quad (67)$$

where the parameter

$$w = -\frac{2\Xi_u}{\lambda_1\sqrt{3}}v_\epsilon \quad (68)$$

controls the detuning from the avoided-crossing resonance due to strain and/or Stark effects. The energies of the pairs of states near the two avoided crossing points equal

$$E_{\pm\frac{1}{2}}^\sigma = \pm \frac{\hbar\omega}{2} + \frac{\sigma\lambda_1}{2}\sqrt{1+w^2}, \quad (69)$$

where $\sigma=\pm 1$ is a new *orbital* quantum number (in addition to the spin z -projection $\pm\frac{1}{2}$). The corresponding eigenfunctions are

$$|\Psi^\sigma, \pm\frac{1}{2}\rangle = \left(\pm i c_\sigma |T_{2x}\rangle + \sqrt{1-c_\sigma^2} |T_{2y}\rangle \right) \otimes |\pm\frac{1}{2}\rangle, \quad (70)$$

where

$$c_\sigma = -\frac{\sigma}{\sqrt{2}} \left[1 - \sigma \frac{w}{\sqrt{1+w^2}} \right]^{1/2}, \quad \sigma = \pm 1. \quad (71)$$

It is of interest to consider the magnetic-dipole transitions between states with opposite spin orientations near the avoided crossing. The matrix elements of the Pauli-matrix $\hat{\sigma}_x$ for spin-flip transitions between states with the same orbital number σ equal

$$\langle \Psi^\sigma, -\frac{1}{2} | \hat{\sigma}_x | \Psi^\sigma, \frac{1}{2} \rangle = \frac{\sigma w}{\sqrt{1+w^2}}, \quad \sigma = \pm 1. \quad (72)$$

It is seen from (69) that the frequencies of these transitions (as well as that of the transition between the states $|E_\epsilon, \pm 1/2\rangle$) are very close to ω forming a triplet of center-lines of magnetic dipole transitions. The matrix elements for spin-flip transitions between states with opposite orbital numbers $\sigma = \pm 1$ equal

$$\langle \Psi^\sigma, -\frac{1}{2} | \hat{\sigma}_x | \Psi^{-\sigma}, \frac{1}{2} \rangle = \frac{1}{\sqrt{1+w^2}} \quad (73)$$

According to (69), the frequencies of these transitions are offset from ω by $\pm\hbar^{-1}\lambda_1\sqrt{1+w^2}$, forming a doublet of satellite lines.

Away from the avoided crossing, $|w| \gg 1$, the matrix elements for transitions between states of the same σ dominate. This behavior can be understood from the fact that, in those regions, each of the hybridized orbitals (70) is dominated by a single orbital character (cf. Fig. 5(b)). Specifically, when $-w \gg 1$,

$$|\Psi^-, \pm\frac{1}{2}\rangle \rightarrow |T_{2y}, \pm\frac{1}{2}\rangle, \quad |\Psi^+, \pm\frac{1}{2}\rangle \rightarrow |T_{2x}, \pm\frac{1}{2}\rangle, \quad (74a)$$

and when $w \gg 1$,

$$|\Psi^-, \pm\frac{1}{2}\rangle \rightarrow |T_{2x}, \pm\frac{1}{2}\rangle, \quad |\Psi^+, \pm\frac{1}{2}\rangle \rightarrow |T_{2y}, \pm\frac{1}{2}\rangle. \quad (74b)$$

Therefore, away from the avoided crossing (i.e. for $|w| \gg 1$) the spin-flip transitions (72) conserving σ are

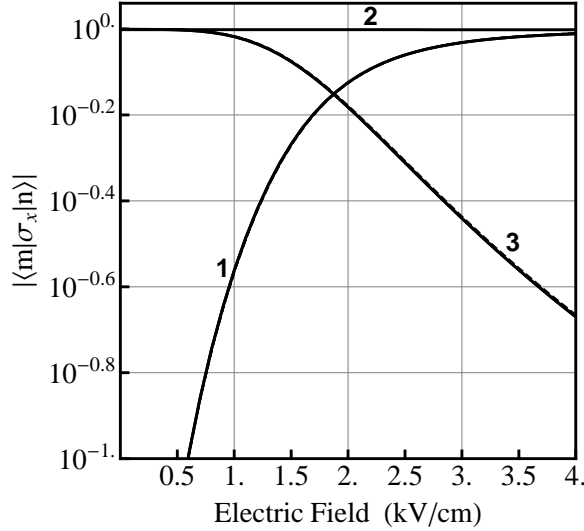


FIG. 7. Matrix elements for the spin-flip transitions vs. electric field near the avoided crossing at $v_\epsilon=0$. Dashed lines (almost undistinguishable in the plots) show the analytical results (72),(73). The lines marked by: (1) correspond to matrix elements for the two direct transitions; (2) correspond to the matrix element for the transition within the Zeeman doublet $|E_\epsilon, \pm 1/2\rangle$ which is very close to 1; and (3) correspond to the matrix elements for the two satellite lines $\Psi_\uparrow^\pm - \Psi_\downarrow^\mp$.

between states with the same dominant orbital character, and the corresponding matrix elements approach unity. At the same time, the transitions in (73) corresponding to satellite lines, are between states with increasingly orthogonal orbital characters as w increases and therefore the corresponding matrix elements approach zero in this limit.

The behavior of the matrix elements for spin-flip transitions at the avoided crossing ($w = 0$) is very different than that away from it. It follows from (70) that at $w=0$ the pairs of states $|\Psi^+, -\frac{1}{2}\rangle, |\Psi^-, +\frac{1}{2}\rangle$ and $|\Psi^-, -\frac{1}{2}\rangle, |\Psi^+, +\frac{1}{2}\rangle$ are, respectively, symmetric and antisymmetric superpositions of the orbital states $i|T_{2x}\rangle$ and $|T_{2y}\rangle$:

$$|\Psi^\mp, \pm\frac{1}{2}\rangle = \frac{i|T_{2x}\rangle + |T_{2y}\rangle}{\sqrt{2}} \otimes |\pm\frac{1}{2}\rangle, \quad (75a)$$

$$|\Psi^\pm, \pm\frac{1}{2}\rangle = \frac{-i|T_{2x}\rangle + |T_{2y}\rangle}{\sqrt{2}} \otimes |\pm\frac{1}{2}\rangle. \quad (75b)$$

The spin-flip transitions (72) that are dominant away from avoided crossing $|w| \gg 1$, connecting the same orbital states, become suppressed at $w = 0$ because they connect the symmetric and antisymmetric superpositions of $i|T_{2x}\rangle$ and $|T_{2y}\rangle$. At the same time, the spin-flip transitions (73) connecting the states with different orbital characters, which are suppressed away from the avoided crossing ($|w| \gg 1$), become dominant at $w = 0$ where they connect the superpositions of $i|T_{2x}\rangle$ and $|T_{2y}\rangle$ with the same symmetry. This behavior is evident from Fig. (7) giving the dependence of matrix elements on elec-

tric field (or effective strain v_ϵ) obtained using the exact numerical solution for the eigenstates of the donor electron Hamiltonian.

There exist four distinct spin-flip transitions between the states of a spin-down doublet Ψ_\downarrow^\pm and those of a spin-up doublet Ψ_\uparrow^\pm . We shall denote the corresponding g -factors as $g_{\sigma,\sigma'}$ ($\sigma, \sigma' = \pm 1$). Based on Eqs. (69) (see also Fig. 5) there are two satellites corresponding to $g_{-,+}$, $g_{-,+}$ and two closely spaced center lines corresponding to $g_{-,-}$, $g_{+,+}$. There is a third center line with g -factor g_{E_ϵ} corresponding to the transition between the states $|E_\epsilon, \pm\frac{1}{2}\rangle$. All g -factors can be obtained by numerical solution of Eq. (62) for the corresponding transitions. The results are shown in Figs. 8.

The numerical results can be very closely approximated analytically when the (xy) -plane strain splitting of T_{2x} , T_{2y} is much smaller than the Zeeman splitting, that is, for $|v_\epsilon| \ll \bar{v}_\epsilon$ (66). We find the coefficients in (64) by a perturbation theory expansion in the spin-orbit interaction constants $\lambda_{1,2}$ using the basis of “correct” states (70) in zeroth order. All five g -factors will have the form

$$g = g_0(1 + \delta) + \Delta_\mu^\eta, \quad (76a)$$

$$\delta = -\frac{1}{3} \left(\epsilon \frac{g_\perp}{g_0} \right) + \frac{1}{8} \left(\frac{\lambda_2}{\hbar\omega_0} \right)^2, \quad (76b)$$

where g_0 is a singlet g -factor and Δ_μ^η corresponds to different shifts for the various g -factors.

For the satellite lines, the shift $\Delta_\sigma^{\text{sat}}$ equals up to the 3rd order in λ_2/ω_0 :

$$\Delta_\sigma^{\text{sat}} = \sigma \frac{g_0 \lambda_1 D(v_\epsilon)}{\hbar\omega_0 - \sigma \lambda_1 D(v_\epsilon)} + \sigma \frac{5}{8} \frac{\lambda_1 \lambda_2^2 D(v_\epsilon)}{(\hbar\omega_0)^3}. \quad (77)$$

Here, we used a secular approximation in (63) keeping the terms linear in λ_1/ω_0 in the denominator because they are proportional to the dimensionless parameter D , which increases away from the avoided crossings

$$D(v_\epsilon) = \sqrt{1 + w^2} = \sqrt{1 + \frac{4}{3} \left(\frac{\Xi_u}{\lambda_1} \right)^2 v_\epsilon^2}, \quad (78)$$

where w is given in (68). At the avoided crossing, g -factor shifts from the centerline $g_0(1 + \delta)$ for satellites are near $2\lambda_1/\hbar\omega_0 \approx 0.13$ (for $\omega_0 = 9600$ MHz). As we discussed previously, while the g -factor shifts for satellite lines increase away from the avoided crossing, the strength of the lines decrease. Note, however, that with detuning from the avoided crossing corresponding to $\mathcal{E} = 3.5$ kV/cm ($v_\epsilon \approx 10^{-6}$) the matrix element is only suppressed by a factor of 4 while the g -factor shift is already of the order of unity. This giant change in g -factor can be seen by comparing the curves $g_{-,+}$ and $g_{+,-}$ in Fig. 8(b), and the curves labeled 3 in Fig. 7.

Fig. 8(a) shows the g -factors $g_{+,+}$, $g_{-,-}$ and g_{E_ϵ} corresponding to three very closely spaced centerlines. Their splitting is not resolved within the 2-level picture near the avoided crossing given by Eqs. (69). We must take

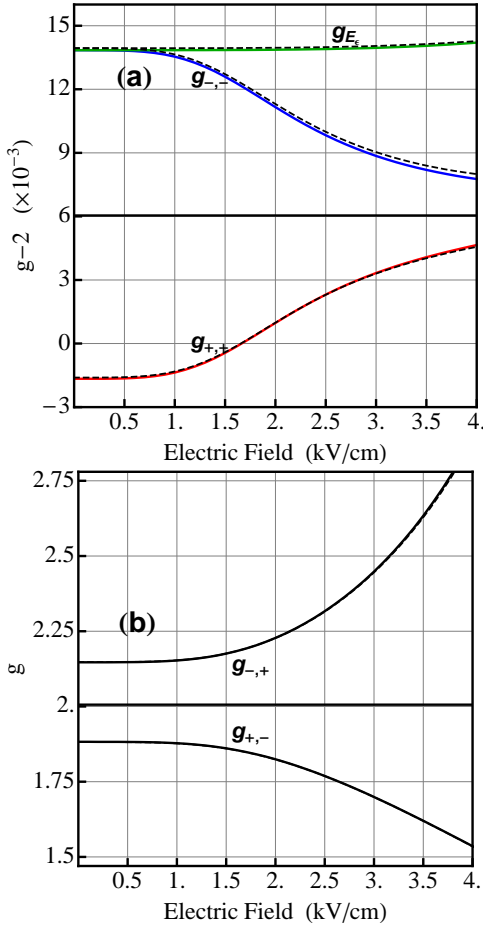


FIG. 8. (Color online.) g -factors vs electric field near the avoided crossing at $v_\epsilon=0$. Figure (a) shows three weakly split center lines, g_{++}, g_{--} and g_{E_ϵ} . Centerline $g_0(1 + \delta)$ (76a) is shown in bold. Figure (b) shows the satellite lines $g_{\pm, \mp}$. Electric field 3.5 kV/cm corresponds approximately to the strain $v_\epsilon \approx 10^{-6}$. Dashed lines (unresolved in some plots) correspond to analytical approximations given in Eqs. (76a), (77), (79) and (80).

into account the transitions between the states $|\Psi_{\uparrow, \downarrow}^\pm\rangle$ and the corresponding states $|E_\epsilon\rangle$ with opposite spin ordination, to determine the splitting. The values of Δ^c give the shifts of three centerlines from the common center. For $g_{\sigma, \sigma}$ ($\sigma=\pm 1$) they are obtained from the expansions of Δ_σ^c in powers of ω_0^{-1} :

$$\Delta_\sigma^c \simeq -\frac{\sigma\lambda_2^2}{4\hbar^2\omega_0^2D} + \frac{\lambda_2^2(D-\sigma)(D^3\lambda_1^2 + (D-\sigma)\lambda_2^2)}{16D^2\omega_0^4\hbar^4}. \quad (79)$$

Here $\sigma = \pm$ and D (78) is a dimensionless detuning from resonance. Note a slight asymmetry between the line shifts that occurs in the 4th order in $\lambda_2/\hbar\omega_0$. Analytical expressions match very closely exact numerical results as demonstrated in Fig. 8(a) where analytical results are shown with dashed lines. The g -factor shift for the tran-

sitions between the $|E_\epsilon, \pm 1/2\rangle$ states equals

$$\Delta_{E_\epsilon}^c = \frac{\lambda_2^2}{4\hbar^2\omega_0^2} + \frac{\lambda_2^2(D^2\lambda_1^2 + 2\lambda_2^2)}{8\hbar^4\omega_0^4}. \quad (80)$$

Note that the dependence of this g -factor on the effective strain variable v_ϵ occurs only in the 4th order in $\lambda_2/\hbar\omega_0$ leading to its slight decrease with v_ϵ also shown in Fig. 8(a). In the leading order, g -factor shifts are symmetric: $\Delta_+^c \simeq -\Delta_-^c$. At the avoided crossing ($D = 1$), g -factor shifts Δ_+^c and $\Delta_{E_\epsilon}^c$ nearly coincide as can also be seen in Fig. 8(a). Away from the avoided crossing $D \gg 1$, the lines Δ_\pm^c asymptotically approach each other as they are shifted down by $(\lambda_2/\hbar\omega_0)^2/4 \approx 0.0076$ from the line $\Delta_{E_\epsilon}^c$. We finally note that in the expressions above (77), (79), (80), we have replaced the singlet g -factor g_0 with the integer value 2.

The above predictions can be better understood and visualized if we plot the ESR lineshapes for different electric fields. Microwave fields stimulate the spin-flip transitions, with resonance emerging as a decrease of the intensity of the received microwave field. The ESR lineshape results are predicted through a simple Lorentzian model. To account for thermal excitation, we assume that the total contribution to the ESR lineshape from a single donor exposed to microwave light of frequency ω_0 will take the form of

$$\varkappa(\mathbf{B}, \boldsymbol{\mathcal{E}}, \mathbf{e}) = \mathcal{Z}^{-1} \sum_{q,r>q} e^{-E_q/k_B T} \varkappa_{qr}(\mathbf{B}, \boldsymbol{\mathcal{E}}, \mathbf{e}), \quad (81)$$

where $\mathcal{Z} = \sum_n \exp(-E_n/k_B T)$. Here \varkappa_{qr} is the lineshape of a single spin-flip transition between the states denoted as q and r . The single-transition contribution reads

$$\varkappa_{qr}(\mathbf{B}, \boldsymbol{\mathcal{E}}, \mathbf{e}) = \frac{1}{2\pi} \frac{4\omega_0\Gamma |\chi_{qr}(\mathbf{B}, \boldsymbol{\mathcal{E}}, \mathbf{e})|^2}{\Gamma^2 + [\omega_0 - \Delta_{rq}(\mathbf{B}, \boldsymbol{\mathcal{E}}, \mathbf{e})]^2}, \quad (82)$$

where $\Delta_{rq} = (E_r - E_q)/\hbar$ and $\chi_{qr} = \langle q | \hat{\sigma}_x | r \rangle$ is the spin-flip transition amplitude between these two states. The parameter Γ expresses the degree of line-broadening due to dispersive mechanisms such as thermal effects and spontaneous phonon emission.

Away from the circled avoided crossings in Fig. 6, the transitions are strongest between the states of the same orbital character. At an electric field of 3 kV/cm, we would expect to see three strong absorption lines corresponding to the three resonant transitions between $|T_{2x}, \uparrow\rangle \leftrightarrow |T_{2x}, \downarrow\rangle$, $|T_{2y}, \uparrow\rangle \leftrightarrow |T_{2y}, \downarrow\rangle$, and $|E_\epsilon, \uparrow\rangle \leftrightarrow |E_\epsilon, \downarrow\rangle$. At the avoided crossing with $v_\epsilon = 0$, a very different situation will be in effect. The transition corresponding to T_{2x} and T_{2y} is suppressed, and new transitions with greatly shifted g -factors will emerge. In the above nomenclature, the transitions corresponding to the g -factors $g_{+,+}$ and $g_{-,-}$ are suppressed in favor of satellite transitions corresponding to $g_{+,-}$ and $g_{-,+}$. The satellite transitions are very sensitive to the random strains, which implies that the likelihood of their detection is extremely low. For this reason we will concentrate on the centerlines and their electric field dependencies.

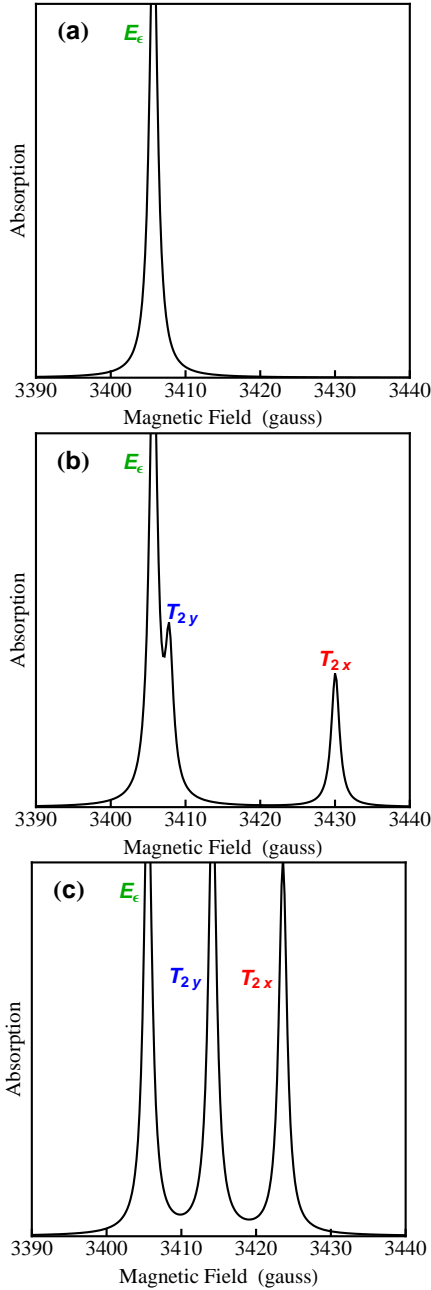


FIG. 9. (Color online.) Modeled ESR lineshape (9600 MHz cavity mode, 1.3 gauss FWHM, 4 Kelvin) for different \mathcal{E} -fields along [100]: (a) $\mathcal{E}=0$, (b) $\mathcal{E}=1.5$ kV/cm, and (c) $\mathcal{E}=3$ kV/cm. The emergence and shifts of T_{2x} and T_{2y} ESR lines are clearly seen.

The g -factor control emerges as the ability to selectively turn these lines “on” and “off”, and to shift the lines themselves. Fig. 9 shows the predictions of our model. The suppression of the two centerlines T_{2y} and T_{2x} at zero field, i.e. near the avoided crossing $v_\epsilon = 0$, and their emergence at higher fields can be clearly seen. The zero-field suppression of the lines is due to the spin-orbit interaction. The two lines emerge because the electric field shifts the energy levels away from the avoided

crossing where the influence of the spin-orbit coupling is much weaker. The overall dependence of the intensity of T_{2x} and T_{2y} lines on the electric field closely follows that of the spin-flip matrix element shown in Fig. 7. As we see in Fig. 9, in the absence of random strain the Stark effect induces a dramatic shift of the ESR lines on the order of 10 gauss.

In Figs 10 and 11, we show the effects of random strains upon the ESR lineshapes and predicted Stark shifts of Li-donor g -factors. We assume that the experimental ESR signal $\bar{\chi}$ can be modeled as an ensemble average over the Gaussian distribution of the random strains:

$$\bar{\chi}(\mathbf{B}, \mathcal{E}) = \int n(\mathbf{e})\chi(\mathbf{B}, \mathcal{E}, \mathbf{e}) d\mathbf{e}. \quad (83)$$

Here $n(\mathbf{e})$ is the Gaussian distribution function and the integration is taken over the strain variables e_θ and e_ϵ . We further assume that a strong uniaxial tensile stress is applied to the sample, and the random internal strains shifting e_θ will have a negligible contribution to the overall ESR signal, i.e. may be safely ignored. Thus we consider only the effect of random variations of e_ϵ , assuming they are described by the Gaussian distributions with different standard deviations (uncertainties) Δe_ϵ .

To better understand the random strain effects presented in Figs. 10 and 11, let us recall our previous finding that the electric field can strongly affect the Zeeman splittings of the centerlines only in the vicinity of the avoided crossings (Fig. 6). In the domain of random strains with Δe_ϵ not exceeding 10^{-7} , most of the donors reside near the avoided crossing $v_\epsilon = 0$. Thus, for the majority of these donors, the centerline transitions T_{2y} and T_{2x} will be suppressed at $\mathcal{E}=0$; however these transitions will emerge for \mathcal{E} -fields exceeding 1 kV/cm. At $\mathcal{E}=3$ kV/cm, the donor spectra will be shifted from $v_\epsilon = 0$ to v_ϵ , exceeding the standard deviation Δe_ϵ . As a result, we see pronounced Stark shifts of the ESR lines on the order of 10 gauss (see Fig. 9 and the top panel of Fig. 10).

The strain disorder randomly shifts the spectra of individual donors away from the avoided crossing $v_\epsilon = 0$. For broad distributions most of the donors are subject to the random strains e_ϵ that exceed v_ϵ corresponding to $\mathcal{E}=3$ kV/cm. The g -factors of these donors are saturated and are insensitive to the applied \mathcal{E} -field (see Fig. 8 (a)). As a result, the majority of the Li spins do not display any significant line shifts induced by the electric field, and the Stark features are washed out of the average signal of the ensemble. As we see from the bottom panel of Fig. 10, for $\Delta e_\epsilon = 5 \cdot 10^{-7}$, the two lines T_{2x} and T_{2y} already exist at $\mathcal{E}=0$, which means they are induced by the random strain. The latter also broadens the lines and pins them down at the zero-field positions. In the domain of larger random strains $\Delta e_\epsilon > 5 \cdot 10^{-7}$ the two lines will merge, broaden and eventually collapse, resulting in a spectrum insensitive to the electric field, with one narrow line E_ϵ . The electric field dependencies of the average g -factors corresponding to different Δe_ϵ (Fig. 11) clearly display flattening with increase of Δe_ϵ .

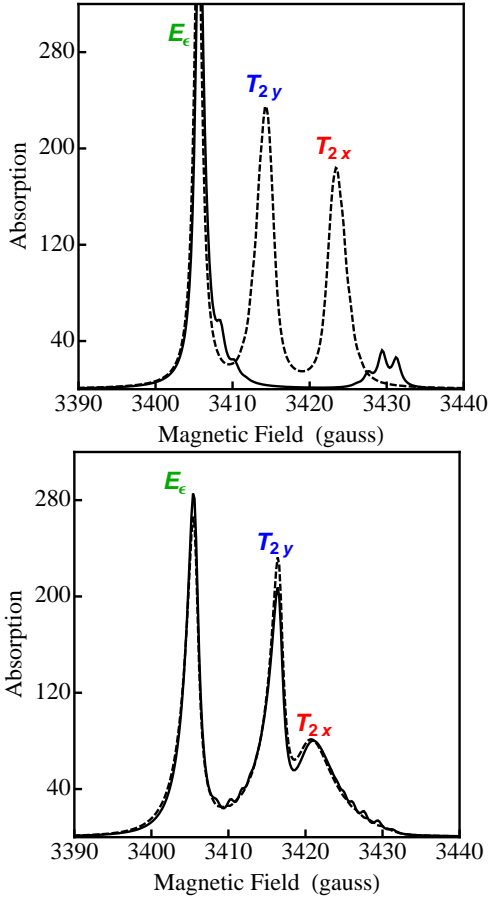


FIG. 10. (Color online.) ESR absorption lineshapes near $v_e = 0$ for different levels of the random strains and different electric fields \mathcal{E} . The solid and dashed lines represent the lineshapes at $\mathcal{E} = 0$ and $\mathcal{E} = 3$ kV/cm respectively. The Stark shifts are prominent for $\Delta e_\epsilon = 10^{-7}$ (top panel) but are almost entirely washed out for $\Delta e_\epsilon = 5 \cdot 10^{-7}$ (bottom panel).

The typical values of the random strain uncertainties Δe_ϵ , which allow for observation of appreciable Stark shifts in Li-doped Si, should be in the range of $\Delta e_\epsilon \sim 10^{-7}$ (Fig. 10). While this requirement is very stringent, the possibility of the growth of low-random-strain Si materials has been demonstrated in photoluminescence experiments³⁹ with ^{28}Si epilayers grown on natural silicon substrates. Yang *et al.*³⁹ were able to resolve splitting of bound exciton lines due to the lattice constant mismatch $\Delta a/a \sim 10^{-6}$ between the epilayer and the substrate. The observed exciton linewidths are at least an order of magnitude smaller than the splitting, which is indicative of the required level of the random strains $\sim 10^{-7}$. The latter are most likely caused by isoelectronic impurities or complexes (e.g. carbon⁴⁰), which implies that the chemical purity of the material is a key factor in reducing these strains.

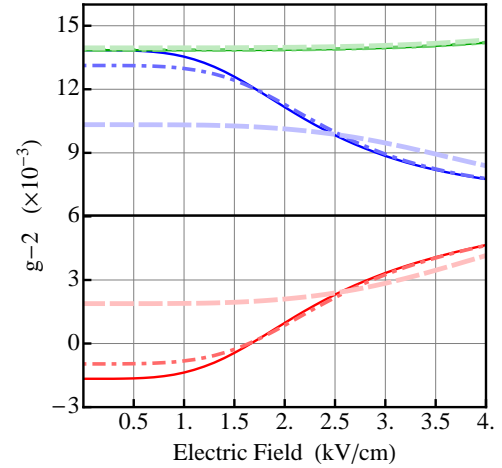


FIG. 11. (Color online.) Stark shifts of electron g -factors for different levels of the random strain. The solid lines are the exact g -factors at zero random strain, shown before in Fig. 8. The dot-dashed lines correspond to $\Delta e_\epsilon = 10^{-7}$ and the dashed lines represent the case of $\Delta e_\epsilon = 5 \cdot 10^{-7}$.

VIII. SUMMARY AND DISCUSSION

We have developed a theory for the Stark effect for lithium donor spins in silicon. The anisotropy of the effective mass leads to the anisotropy of the quadratic Stark susceptibility, which we determined using the Dalgarno-Lewis exact summation method³⁶. The theory is asymptotically exact in the field domain below Li-donor ionization threshold, relevant to the Stark-tuning ESR experiments¹⁹. Using this theory as a calibration tool we devised a new variational wave function for a shallow donor in the electric field. The variational function replicates the exact small-field asymptotic results and is robust for large fields.

With the calculated Stark susceptibilities and the new variational function at hand, we predicted and analyzed several important physical effects. First, we observed that the energy level shifts due to the quadratic Stark effect are equivalent to and can be mapped onto those produced by an external stress³. Second, we demonstrated that the Stark effect anisotropy, combined with unique valley-orbit splitting of a Li donor in Si, spin-orbit interaction and specially tuned external stress, may lead to a very strong modulation of the donor spin g -factor by the electric field. Third, we investigated the influence of random strains on the g -factor shifts and quantified the random strain limits which are necessary to observe the ESR-Stark shifts experimentally.

The ability to control g -factors with electric field and/or stress is a crucial component of many solid-state based quantum computing schemes.^{1,5-7} Of particular interest for QIP proposals is the situation that emerges when states with opposite spin-orientations are allowed to mix through the spin-orbit interaction leading to the avoided crossings. This has implications not only for g -

factor control but also for long-range inter-donor elastic-dipole coupling, suggesting the possibility of controllable interactions between isolated donor qubits.² Both of these capabilities can be utilized to implement a universal set of gates based on the Ising Hamiltonian.⁴¹ This would require ability to grow Si multilayer structures with a given value of the in-plane strain. The promising technique, which can be used for practical purposes of achieving precise control of the uniaxial and/or biaxial strain, is the growth of Si films on compliant surfaces.⁴² Another interesting possibility is the utilization of piezo-actuators to implement local stress control of individual

impurities.⁴³

ACKNOWLEDGMENTS

This work was supported by NASA Cooperative Agreement NNX10AJ58A, the United States National Security Agency, DOE Grant No. de-sc0004890, and the Mines Medal Fellowship (E. M. Handberg).

Appendix A: Derivation of Eqs. (19)

We seek to solve the differential problem

$$\left(\nabla^2 - 2\frac{\partial}{\partial r}\right) \mathbf{f} - \lambda \left(\frac{\partial^2}{\partial z^2} - 2\frac{z}{r}\frac{\partial}{\partial z}\right) \mathbf{f} = -\frac{2m_{\perp}a_{\perp}^3}{\hbar^2} \boldsymbol{\zeta}, \quad (\text{A1})$$

where $\boldsymbol{\zeta} = (x, y, za_{\parallel}/a_{\perp})$. First, we use the product rules

$$\nabla^2 (\cos(\phi)f(r, \theta)) = \cos \phi \left(\nabla^2 - \frac{1}{r^2 \sin^2 \theta}\right) f(r, \theta), \quad (\text{A2a})$$

$$\frac{\partial}{\partial z} (\cos(\phi)f(r, \theta)) = \cos \phi \frac{\partial f}{\partial z}, \quad (\text{A2b})$$

and similar rules for the derivatives of $\sin \phi \cdot f(r, \theta)$. If we substitute \mathbf{f} in the form of Eqs. (16) into Eq. (A1) and use the rules (A2) we are able to separate the ϕ dependence and obtain partial differential equations for $f_{\parallel}(r, \theta)$ and $f_{\perp}(r, \theta)$ as follows:

$$\left(\nabla^2 - 2\frac{\partial}{\partial r}\right) f_{\parallel} - \lambda \left(\frac{\partial^2}{\partial z^2} - 2\frac{z}{r}\frac{\partial}{\partial z}\right) f_{\parallel} = -r \cos \theta, \quad (\text{A3a})$$

$$\left(\nabla^2 - \frac{1}{r^2 \sin^2 \theta} - 2\frac{\partial}{\partial r}\right) f_{\perp} - \lambda \left(\frac{\partial^2}{\partial z^2} - 2\frac{z}{r}\frac{\partial}{\partial z}\right) f_{\perp} = -r \sin \theta. \quad (\text{A3b})$$

These equations can be further simplified by employing product rules involving the associated Legendre polynomials

$$\left(\nabla^2 - \frac{m^2}{r^2 \sin^2 \theta}\right) f(r)P_l^m(\cos \theta) = P_l^m(\cos \theta) \left[\nabla^2 - \frac{l(l+1)}{r^2}\right] f(r), \quad (\text{A4})$$

and substituting Eqs. (17) into Eqs. (A3). This yields:

$$\sum_l P_l(\cos \theta) \left(r^2 \hat{D}_r - l(l+1)\right) f_{\parallel, l} = \lambda r^2 \sum_l \hat{D}_z(f_{\parallel, l} P_l(\cos \theta)) - r^3 \cos \theta \quad (\text{A5a})$$

$$\sum_l P_l^1(\cos \theta) \left(r^2 \hat{D}_r - l(l+1)\right) f_{\perp, l} = \lambda r^2 \sum_l \hat{D}_z(f_{\perp, l} P_l^1(\cos \theta)) + r^3 \sin \theta \quad (\text{A5b})$$

where \hat{D}_r and \hat{D}_z are defined in Eqs. (15).

If $\lambda = 0$, Eqs. (A5) have particular solutions $f_{\parallel} = f(r) \cos \theta$ and $f_{\perp} = f(r) \sin \theta$. Indeed, we obtain an ordinary differential equation for $f(r)$

$$r^2 \frac{d^2 f}{dr^2} + 2r(1-r) \frac{df}{dr} - 2f = -r^3, \quad (\text{A6})$$

which has the particular solution

$$f(r) = \frac{r(r+2)}{4}. \quad (\text{A7})$$

The operator \hat{D}_z mixes the Legendre polynomials with different l and does not allow to separate r and θ . However, the problem can be reduced to a chain of coupled

ordinary differential equations. To proceed, we employ another set of rules:

$$\frac{\partial}{\partial z} f(r) P_l^m(\cos \theta) = \cos(\theta) P_l^m \frac{\partial f}{\partial r} - \frac{f}{r} \sin(\theta) \frac{\partial P_l^m}{\partial \theta}, \quad (\text{A8a})$$

$$\cos(\theta) P_l^m = \frac{l+m}{2l+1} P_{l-1}^m + \frac{l-m+1}{2l+1} P_{l+1}^m, \quad (\text{A8b})$$

$$\sin(\theta) \frac{\partial P_l^m}{\partial \theta} = -\frac{(l+1)(l+m)}{2l+1} P_{l-1}^m + \frac{l(l-m+1)}{2l+1} P_{l+1}^m. \quad (\text{A8c})$$

We use these rules to rewrite $r^2 \hat{D}_z f_l(r) P_l^m(\cos \theta)$ as

$$r^2 \hat{D}_z (f_l(r) P_l^m(\cos \theta)) = \left(P_{l-2}^m \hat{\alpha}_{l-2}^m + P_l^m \hat{\beta}_l^m + P_{l+2}^m \hat{\gamma}_{l+2}^m \right) f_l(r), \quad (\text{A9})$$

where $\hat{\alpha}_l^m, \hat{\beta}_l^m, \hat{\gamma}_l^m$ are second order radial differential operators having a common structure of Eq. (20) with the coefficients $\alpha_{l,m}^{(i)}, \beta_{l,m}^{(i)}$ and $\gamma_{l,m}^{(i)}$ given explicitly as

$$\alpha_{l,m}^{(0)} = \frac{(l+m+1)(l+m+2)}{(2l+3)(2l+5)} \quad (\text{A10a})$$

$$\alpha_{l,m}^{(1)} = 2l+5 \quad (\text{A10b})$$

$$\alpha_{l,m}^{(2)} = -2(l+3) \quad (\text{A10c})$$

$$\alpha_{l,m}^{(3)} = (l+1)(l+3) \quad (\text{A10d})$$

$$\beta_{l,m}^{(0)} = \frac{2l^2 + 2l - 2m^2 - 1}{(2l-1)(2l+3)} \quad (\text{A11a})$$

$$\beta_{l,m}^{(1)} = 2 \quad (\text{A11b})$$

$$\beta_{l,m}^{(2)} = -1 + \frac{4m^2 + 1}{2l^2 + 2l - 2m^2 - 1} \quad (\text{A11c})$$

$$\beta_{l,m}^{(3)} = l(l+1) \quad (\text{A11d})$$

$$\gamma_{l,m}^{(0)} = \frac{(l-m)(l-m-1)}{(2l-1)(2l-3)} \quad (\text{A12a})$$

$$\gamma_{l,m}^{(1)} = -2l+3 \quad (\text{A12b})$$

$$\gamma_{l,m}^{(2)} = 2(l-2) \quad (\text{A12c})$$

$$\gamma_{l,m}^{(3)} = l(l-2) \quad (\text{A12d})$$

We then multiply both sides of Eqs. (A5) by $P_l^m(\cos \theta) \sin \theta$ and integrate $\int_0^\pi d\theta \sin(\theta) P_l^m(\cos \theta) \dots$, to eliminate θ -dependence at the expense of mixing f_l with different values of l . This procedure leads to Eqs (19).

Appendix B: Spectrum Narrowing Effect

The matrix of the central cell potential in the basis of valley-orbitals reads:

$$H'_{vo} = \begin{pmatrix} \Delta_{0x} & \Delta_{1x} & \Delta_{2xy} & \Delta_{2xy} & \Delta_{2xz} & \Delta_{2xz} \\ \Delta_{1x} & \Delta_{0x} & \Delta_{2xy} & \Delta_{2xy} & \Delta_{2xz} & \Delta_{2xz} \\ \Delta_{2xy} & \Delta_{2xy} & \Delta_{0y} & \Delta_{1y} & \Delta_{2yz} & \Delta_{2yz} \\ \Delta_{2xy} & \Delta_{2xy} & \Delta_{1y} & \Delta_{0y} & \Delta_{2yz} & \Delta_{2yz} \\ \Delta_{2xz} & \Delta_{2xz} & \Delta_{2yz} & \Delta_{2yz} & \Delta_{0z} & \Delta_{1z} \\ \Delta_{2xz} & \Delta_{2xz} & \Delta_{2yz} & \Delta_{2yz} & \Delta_{1z} & \Delta_{0z} \end{pmatrix}. \quad (\text{B1})$$

Transforming this the symmetrized-orbital basis, we find

$$H_{vo} = \begin{pmatrix} D_A & A & B & 0 & 0 & 0 \\ A & D_{E\theta} & C & 0 & 0 & 0 \\ B & C & D_{E\epsilon} & 0 & 0 & 0 \\ 0 & 0 & 0 & D_x & 0 & 0 \\ 0 & 0 & 0 & 0 & D_y & 0 \\ 0 & 0 & 0 & 0 & 0 & D_z \end{pmatrix} \quad (\text{B2})$$

Here the energy zero is shifted to the ‘‘center of gravity’’ of the manifold. Explicit expressions for the diagonal matrix elements are

$$D_A = \frac{1}{3} (\Delta_{1x} + \Delta_{1y} + \Delta_{1z} + 4\Delta_{2xy} + 4\Delta_{2xz} + 4\Delta_{2yz}), \quad (\text{B3a})$$

$$D_{E\theta} = -\frac{1}{6} (\Delta_{0x} + \Delta_{0y} - 2\Delta_{0z} - \Delta_{1x} - \Delta_{1y} - 4\Delta_{1z} - 4\Delta_{2xy} + 8\Delta_{2xz} + 8\Delta_{2yz}), \quad (\text{B3b})$$

$$D_{E\epsilon} = \frac{1}{6} (\Delta_{0x} + \Delta_{0y} - 2\Delta_{0z} + 3\Delta_{1x} + 3\Delta_{1y} - 12\Delta_{2xy}), \quad (\text{B3c})$$

$$D_x = \frac{1}{3} (2\Delta_{0x} - \Delta_{0y} - \Delta_{0z} - 3\Delta_{1x}), \quad (\text{B3d})$$

$$D_y = \frac{1}{3} (2\Delta_{0y} - \Delta_{0x} - \Delta_{0z} - 3\Delta_{1y}), \quad (\text{B3e})$$

$$D_z = \frac{1}{3} (2\Delta_{0z} - \Delta_{0x} - \Delta_{0y} - 3\Delta_{1z}). \quad (\text{B3f})$$

Similarly, the non-diagonal matrix elements can be expressed as

$$A = -\frac{\sqrt{2}}{6} (\Delta_{0x} + \Delta_{0y} - 2\Delta_{0z} + \Delta_{1x} + \Delta_{1y} - 2\Delta_{1z} + 4\Delta_{2xy} - 2\Delta_{2xz} - 2\Delta_{2yz}), \quad (\text{B3g})$$

$$B = \frac{\sqrt{6}}{6} (\Delta_{0x} - \Delta_{0y} + \Delta_{1x} - \Delta_{1y} + 2\Delta_{2xz} - 2\Delta_{2yz}), \quad (\text{B3h})$$

$$C = -\frac{\sqrt{3}}{6} (\Delta_{0x} - \Delta_{0y} + \Delta_{1x} - \Delta_{1y} - 4\Delta_{2xz} + 4\Delta_{2yz}). \quad (\text{B3i})$$

At zero electric field, $F_x = F_y = F_z = F_0$. Using these values in Eqs. (39a)–(39c), and substituting them into

the matrix (B2), we find the zero-field valley-orbit Hamiltonian to be

$$H_{vo}^{(0)} = \begin{pmatrix} D_A^{(0)} & 0 & 0 & 0 & 0 & 0 \\ 0 & D_E^{(0)} & 0 & 0 & 0 & 0 \\ 0 & 0 & D_E^{(0)} & 0 & 0 & 0 \\ 0 & 0 & 0 & D_T^{(0)} & 0 & 0 \\ 0 & 0 & 0 & 0 & D_T^{(0)} & 0 \\ 0 & 0 & 0 & 0 & 0 & D_T^{(0)} \end{pmatrix}, \quad (\text{B4})$$

where each term on the diagonal is such that

$$D_A^{(0)} = F_0^2(\nu_1 + 4\nu_2), \quad (\text{B5a})$$

$$D_E^{(0)} = F_0^2(\nu_1 - 2\nu_2), \quad (\text{B5b})$$

$$D_T^{(0)} = -F_0^2\nu_1. \quad (\text{B5c})$$

We identify each term on the diagonal with the singlet, doublet, and triplet binding energies of the $1s$ donor manifold. Since these values are well known from experiment, we can use the constants ν_0 , ν_1 , ν_2 to reproduce the spectrum of any shallow donor in Si.

The spectrum narrowing Hamiltonian is defined by $H_{sn} = H_{vo} - H_{vo}^{(0)}$. To evaluate the extent of spectrum narrowing due to displacement of the electron away from the donor site, we write

$$F_j = F_0(1 + \delta_j), \quad (\text{B6})$$

where δ_j is a function of the field. The values of δ_j can be obtained variationally. Our analysis yields

$$\delta_j = \frac{1}{2}(f_{\perp}^{(2)} - f_{\parallel}^{(2)})\mathcal{E}_j^2 - \frac{1}{2}f_{\perp}^{(2)}\mathcal{E}^2, \quad (\text{B7})$$

where \mathcal{E}_j is the component of the field lying along the i th valley. For fields up to 10 kV/cm, the values of δ

remain below 0.02. In the valley-orbit matrix the couplings are $\Delta_{0j} = \nu_0 F_0^2(1 + 2\delta_j)$, $\Delta_{1j} = \nu_1 F_0^2(1 + 2\delta_j)$, $\Delta_{2ij} = \nu_2 F_0^2(1 + \delta_i + \delta_j)$ where the terms to the first order in δ (second order in \mathcal{E}) are retained.

To simplify the matrix expressions, we express for our valley-orbit matrix in terms of δ_i . Then the spectrum narrowing Hamiltonian matrix can be written as the sum of three simpler matrices

$$H_{sn} = F_0^2 \left(\delta_{\theta} \hat{U}_{\theta} + \delta_{\epsilon} \hat{U}_{\epsilon} + \delta_{\eta} \hat{U}_{\eta} \right). \quad (\text{B8})$$

The parameters δ_{μ} , determining the strength of the narrowing, are given by

$$\delta_{\theta} = \frac{1}{3}(-\delta_x - \delta_y + 2\delta_z), \quad (\text{B9a})$$

$$\delta_{\epsilon} = \frac{\sqrt{3}}{3}(\delta_x - \delta_y), \quad (\text{B9b})$$

$$\delta_{\eta} = \delta_x + \delta_y. \quad (\text{B9c})$$

The component matrices may be expressed in the in the symmetrized-orbital basis

$$\begin{aligned} \hat{U}_{\theta} = & (\nu_1 + 4\nu_2) |A_1\rangle \langle A_1| + (\nu_0 + 2\nu_1 - 4\nu_2) |E_{\theta}\rangle \langle E_{\theta}| \\ & + (2\nu_0 - 3\nu_1) |T_{2z}\rangle \langle T_{2z}| + \nu_{\alpha} |A_1\rangle \langle E_{\theta}| + H.C. \\ & - \nu_{\theta} (|E_{\epsilon}\rangle \langle E_{\epsilon}| + |T_{2x}\rangle \langle T_{2x}| + |T_{2y}\rangle \langle T_{2y}|) \end{aligned} \quad (\text{B10a})$$

$$\begin{aligned} \hat{U}_{\epsilon} = & \sqrt{3}(\nu_0 - \nu_1) (|T_{2x}\rangle \langle T_{2x}| - |T_{2y}\rangle \langle T_{2y}|) \\ & - \nu_{\theta} |E_{\theta}\rangle \langle E_{\theta}| + \nu_{\alpha} |A_1\rangle \langle E_{\epsilon}| + H.C. \end{aligned} \quad (\text{B10b})$$

$$\begin{aligned} \hat{U}_{\eta} = & -\nu_1 (|T_{2x}\rangle \langle T_{2x}| + |T_{2y}\rangle \langle T_{2y}| + |T_{2z}\rangle \langle T_{2z}|) \\ & + (\nu_1 - 2\nu_2) (|E_{\theta}\rangle \langle E_{\theta}| + |E_{\epsilon}\rangle \langle E_{\epsilon}|) \\ & + (\nu_1 + 4\nu_2) |A_1\rangle \langle A_1| \end{aligned} \quad (\text{B10c})$$

with $\nu_{\alpha} = \sqrt{2}(\nu_0 + \nu_1 + \nu_2)$, and $\nu_{\theta} = \nu_0 + \nu_1 - 2\nu_2$.

-
- * Andre.Petukhov@sdsmt.edu
- ¹ B. Kane, Nature **393**, 133 (1998).
 - ² V. Smelyanskiy, A. Petukhov, and V. Osipov, Phys. Rev. B **72**, 081304 (2005).
 - ³ G. Watkins and F. Ham, Phys. Rev. B **1**, 4071 (1970).
 - ⁴ C. Jagannath and A. Ramdas, Phys. Rev. B **23**, 4426 (1981).
 - ⁵ D. Loss and D. P. DiVincenzo, Phys. Rev. A **57**, 120 (1998).
 - ⁶ R. Vrijen, E. Yablonovitch, K. Wang, H. W. Jiang, A. Balandin, V. Roychowdhury, T. Mor, and D. DiVincenzo, Phys. Rev. A **62**, 012306 (2000).
 - ⁷ H. Jiang and E. Yablonovitch, Phys. Rev. B **64**, 041307 (2001).
 - ⁸ Y. Kato, R. C. Myers, D. C. Driscoll, A. C. Gossard, J. Levy, and D. D. Awschalom, Science **299**, 1201 (2003).
 - ⁹ I. Žutić, J. Fabian, and S. Das Sarma, Rev. Mod. Phys. **76**, 323 (2004).
 - ¹⁰ J. R. Petta, A. C. Johnson, J. M. Taylor, E. A. Laird, A. Yacoby, M. D. Lukin, C. M. Marcus, M. P. Hanson, and A. C. Gossard, Science **309**, 2180 (2005).
 - ¹¹ Y. Tokura, W. van der Wiel, T. Obata, and S. Tarucha, Phys. Rev. Lett. **96**, 047202 (2006).
 - ¹² T. Nakaoka, S. Tarucha, and Y. Arakawa, Phys. Rev. B **76**, 041301 (2007).
 - ¹³ K. C. Nowack, F. H. L. Koppens, Y. V. Nazarov, and L. M. K. Vandersypen, Science **318**, 1430 (2007).
 - ¹⁴ E. Laird, C. Barthel, E. Rashba, C. Marcus, M. Hanson, and A. Gossard, Phys. Rev. Lett. **99**, 246601 (2007).
 - ¹⁵ M. Piore-Ladrière, T. Obata, Y. Tokura, Y. S. Shin, T. Kubo, K. Yoshida, T. Taniyama, and S. Tarucha, Nature Phys. **4**, 776 (2008).
 - ¹⁶ S. Nadj-Perge, S. M. Frolov, E. P. A. M. Bakkers, and L. P. Kouwenhoven, Nature **468**, 1084 (2010).
 - ¹⁷ M. Shafiei, K. C. Nowack, C. Reichl, W. Wegscheider, and L. M. K. Vandersypen, arXiv:12073331 (2012).
 - ¹⁸ A. De, C. Pryor, and M. Flatté, Phys. Rev. Lett. **102**, 17603 (2009).

- ¹⁹ F. Bradbury, A. Tyryshkin, G. Sabouret, J. Bokor, T. Schenkel, and S. Lyon, *Phys. Rev. Lett.* **97**, 176404 (2006).
- ²⁰ M. Friesen, *Phys. Rev. Lett.* **94**, 186403 (2005).
- ²¹ G. D. J. Smit, S. Rogge, J. Caro, and T. M. Klapwijk, *Phys. Rev. B* **70**, 035206 (2004).
- ²² A. Martins, R. Capaz, and B. Koiller, *Phys. Rev. B* **69** (2004).
- ²³ H. Hasegawa, *Phys. Rev.* **118**, 1523 (1960).
- ²⁴ L. Roth, *Phys. Rev.* **118**, 1534 (1960).
- ²⁵ B. Golding and M. I. Dykman, arXiv:0309147 (2003).
- ²⁶ R. Faulkner, *Phys. Rev.* **184**, 713 (1969).
- ²⁷ D. M. Larsen, *Phys. Rev. B* **67**, 165204 (2003).
- ²⁸ W. Kohn and J. Luttinger, *Phys. Rev.* **98**, 915 (1955).
- ²⁹ G. D. J. Smit, S. Rogge, J. Caro, and T. M. Klapwijk, *Phys. Rev. B* **68**, 193302 (2003).
- ³⁰ R. Rahman, C. J. Wellard, F. R. Bradbury, M. Prada, J. H. Cole, G. Klimeck, and L. C. L. Hollenberg, *Phys. Rev. Lett.* **99**, 036403 (2007).
- ³¹ G. P. Lansbergen, R. Rahman, C. J. Wellard, I. Woo, J. Caro, N. Collaert, S. Biesemans, G. Klimeck, L. C. L. Hollenberg, and S. Rogge, *Nature Phys.* **4**, 656 (2008).
- ³² E. Merzbacher, *Quantum Mechanics* (John Wiley & Sons, New York, 1998), 3rd ed.
- ³³ V. Privman, *Phys. Rev. A* **22**, 1833 (1980).
- ³⁴ G. Alvarez, R. Damburg, and H. Silverstone, *Phys. Rev. A* **44**, 3060 (1991).
- ³⁵ I. Ivanov, *Phys. Rev. A* **56**, 202 (1997).
- ³⁶ A. Dalgarno and J. T. Lewis, *Proc. Roy. Soc. A* **233**, 70 (1955).
- ³⁷ H. Fritzsche, *Phys. Rev.* **125**, 1560 (1962).
- ³⁸ C. Herring and E. Vogt, *Phys. Rev.* **101**, 944 (1956).
- ³⁹ A. Yang, H. Lian, M. Thewalt, M. Uemura, A. Sagara, K. Itoh, E. Haller, J. Ager III, and S. Lyon, *Physica B: Condensed Matter* **376**, 54 (2006).
- ⁴⁰ A. N. Safonov, G. Davies, and E. C. Lightowlers, *Phys. Rev. B* **54**, 4409 (1996).
- ⁴¹ R. De Sousa, J. Delgado, and S. Das Sarma, *Phys. Rev. A* **70**, 052304 (2004).
- ⁴² H. Yin, R. L. Peterson, K. D. Hobart, S. R. Shieh, T. S. Duffy, and J. C. Sturm, *Appl. Phys. Lett.* **87**, 061922 (2005).
- ⁴³ L. Dreher, T. Hilker, A. Brandlmaier, S. Goennenwein, H. Huebl, M. Stutzmann, and M. Brandt, *Phys. Rev. Lett.* **106**, 037601 (2011).